Ain Shams Engineering Journal 15 (2024) 102833

Contents lists available at ScienceDirect

Ain Shams Engineering Journal

journal homepage: www.sciencedirect.com

Full Length Article

Magnetohydrodynamic flow of carbon nanotubes and heat transfer over a moving thin Needle: A numerical and research surface methodology

Nazrul Azlan Abdul Samat [a,b,*], Norfifah Bachok [a,c,1], Norihan Md Arifin [a,c,1]

[a] Department of Mathematics and Statistics, Faculty of Science, Universiti Putra Malaysia, 43400 UPM Serdang, Selangor, Malaysia
[b] Department of Management, Faculty of Management and Information Technology, Universiti Sultan Azlan Shah, 33000 Kuala Kangsar Perak, Malaysia
[c] Institute for Mathematical Research, Universiti Putra Malaysia, 43400 UPM Serdang, Selangor, Malaysia

ARTICLE INFO

Keywords:
CNTs nanofluids flow
Movable thin needle
Magnetohydrodynamic
Multiple solutions
Optimisation

ABSTRACT

A steady flow of carbon nanotubes (CNTs) nanofluids and heat transfer past a horizontally moving thin needle are investigated under the influence of magnetohydrodynamic (MHD). Single-walled CNTs (SWCNTs) and multi-walled CNTs (MWCNTs) are the two main nanoparticles that represent CNTs. The slender needle moves relative to the flow with parallel velocity in either the same or opposite direction. Using the similarity method, a system of partial differential equations (PDEs) subject to boundary conditions is converted into nondimensional ordinary equations (ODEs). The ODEs are then reduced to a first-order ODEs system and solved using the MATLAB R2022b bvp4c solver. On a numerical scale, the impacts of varying potential parameters, such as the magnetic, CNTs' volume fraction, and moving parameters, on the velocity and temperature profiles, the skin friction, and heat transfer coefficients are investigated. Utilising response surface methodology (RSM), the optimisation of the response based on numerical experimentation of physical quantities is performed. The outcomes are depicted using tables and a graphical approach. Results indicate the existence of dual solutions when the needle travels in the opposite direction. Moreover, the increase in the magnetic parameter by 100% in the flow will increase both the skin friction and heat transfer coefficients by nearly 30% and 4%, respectively. Furthermore, when the value of the CNTs volume fraction increases by 100%, the heat transfer rate increases substantially by almost 33%. However, doubling the size of the thin needle can significantly reduce the skin friction coefficient by nearly 32%. RSM results demonstrate that the maximal heat transfer coefficient is generated at the highest values of the magnetic and CNTs' volume friction parameters and the lowest value of the needle size parameter. Findings also show that SWCTNs are superior to MWCNTs both in the skin friction and heat transfer coefficients. When comparing the performance of water and kerosene, we find that water is less effective as a base fluid than kerosene.

1. Introduction

The use of nanofluids (NFs) to enhance the thermal properties of various devices with electronic cooling systems, such as heat exchangers and radiators, intrigues many researchers. As an example of a non-Newtonian fluid, this fluid has thermo-physical features that beat the characteristics of Newtonian liquids, which include water and oil. NFs have been synthesized from various nanomaterials, including metallic (see Refs. [1,2]) and non-metallic materials (see Refs [3,4]), by blending them with a regular fluid using the single- or two-phase method. Ibrahim et al.'s review article [5] provided strong evidence for the claim that NFs have advantageous effects in applications since the first discovery of NFs by Choi and Eastman [6]. This team looked at multiple data sets and came to the conclusion that the thermo-physical properties of NFs, such as their specific heat, viscosity, and thermal conductivity, were great for making the heat transfer process work better. Despite NFs' impressive thermal management performance, Sajid et al. [7] remarked that the intricacy of NFs' viscosity makes it challenging to explain its behaviour using a mathematical approach. Therefore, it becomes essential to construct mathematical models for examining the flow of nanofluids and improving our understanding of their behaviour. In order to provide a range of outcomes and solutions, the model must take into account the fluid motion across various geometric shapes and effects. Several

* Corresponding author.
E-mail addresses: nazrul_lan@usas.edu.my, ilmulight.86@gmail.com (N. Azlan Abdul Samat), norfifah@upm.edu.my (N. Bachok), norihan@upm.edu.my (N. Md Arifin).
[1] Co-author:

https://doi.org/10.1016/j.asej.2024.102833
Received 7 February 2024; Received in revised form 28 March 2024; Accepted 15 April 2024
Available online 26 April 2024

Nomenclature

Pr	Prandtl number
T	Constant temperature
U	Constant velocity
M	Magnetic parameter
c	Needle size
Nu_x	Local Nusselt number
Re_x	Local Reynolds number
C_f	Skin friction coefficient
Res	Response
u, v	Velocity components
x	Axial coordinates
r	Radial coordinates

Subscripts

w	Condition on needle surface
∞	Ambient condition
nf	Nanofluids
f	Base fluid
CNT	Carbon nanotubes
$SWCNT$	Single-walled carbon nanotubes
$MWCNT$	Multi-walled carbon nanotubes
A	Response for SWCNTs
B	Response for MWCNTs

Greek Symbols

α	Thermal diffusivity
μ	Dynamic viscosity
ρ	Density
B	Magnetic field
ψ	Non-dimensional stream function
η	Non-dimensional thickness
C_p	Specific heat
σ	Electrical conductivity
k	Thermal conductivity
A	Distance
ν	Kinematic viscosity
ϕ	CNTs volume fraction
λ	Moving parameter
λ_c	Critical value
$\in$	Error term
α	Thermal diffusivity

researchers, such as those in Refs. [8–13], have accomplished their goal of creating mathematical models for nanofluids flow. To build models, scientists have been utilised various nanofluids models, including Buongiorno's model (see Refs. [14–17]) and Tiwari and Das's model (see Refs. [18–22]).

Concerns about mitigating climate change have increased demand for products that are favourable to the environment. However, scientists have encountered challenges in selecting eco-friendly nanomaterials for the preparation of NFs in order to promote green applications. With variations of nanomaterials from metallic, non-metallic, and carbon-based, NFs can work effectively by dispersing them in based fluids. According to various investigations, carbon nanotubes (CNTs) have been identified as one of the most promising candidates for environmentally harmless nanoparticles. Recent research by Mahmood et al. [23] indicated that CNTs have been the most developed nanostructures for more than two decades due to their wide availability on earth and eco-friendliness.

Besides, CNTs also have excellent physical and thermal characteristics, as Aladag et al. [24] showed experimentally the advantages of using CNTs in water-based systems for generating a high shear rate. The other experimental work performed by Arya et al. [25] demonstrated an increase in the heat transfer coefficient by incorporating CNTs nanofluids into the cooling system. Hence, to prepare productive and eco-friendly nanofluids for heat transfer applications, CNTs should be selected as the nanoparticles of highest preference.

Ijima [26] created the first multi-walled carbon nanotubes (MWCNTs) in 1991 and single-walled carbon nanotubes (SWCNTs) two years later. SWCNTs and MWCNTs have grown to be the most prevalent types of CNTs, with numerous experiments and mathematical models investigating their behaviour. The demand for manipulating them for research purposes has increased as a result of the compelling evidence provided by Afrand et al. and Ali et al. [27,28]. This team listed SWCNTs and MWCNTs at the top of the list of commonly used nanoparticles with thermal conductivities of 6600 (W/m K) and 3000 (W/m K), respectively.

A number of scientists have come up with numerous models of the flow of CNTs nanofluids over diverse geometries and the effects within the flow. Yasir et al. [29] stated that studying the flow across slender needles has become attractive numerical research because laboratory experiments face significant limitations in accurately visualising the velocity and temperature profiles. By implementing a numerical approach, scientists may estimate both profiles, which are key factors in evaluating flow dynamics. Numerous industrial pieces of equipment, including in the biomedical and engineering fields, currently incorporate the use of slender needles. Since Lee [30] was the first to carry out an analytical and numerical investigation of boundary layers over a thin needle in 1967, far too little attention has been paid to the flow of CNTs nanofluids over a thin needle. Souayeh et al. [31] described the thin needle as being an asymmetrically parabolic and curved object. However, Shafiq et al. [32] distinguished the various dimensions of thin needles by proposing three variables of thin needle wall shapes: paraboloid, cone, and cylinder. Utilising SWCNTs suspended in ethylene glycol, this model determined that, when compared to the other needle bodies, the cylindrical needle was the most efficient tool for transferring heat. Contrary to Shafiq et al.'s work [32], Kumar et al. [33] found that the paraboloid surface offered the best heat transfer performance.

Tlili et al. [34] emerged as one of the groups actively investigating the flow of CNTs nanofluids. They made a model of CNTs flow by taking into account the production of entropy and nonlinear thermal radiation in a Darcy-Forchheimer porous medium and assuming that the thin needle is a movable object. Using water as the base fluid, the study discovered that the size of the needle and Hall current parameters affected the velocity profile. Singh et al. [35] also took into account the influence of needle size. Based on this model, the rate of transport was considerably reduced with an increase in the dimensionless needle size, and the shear stress decreased with an increase in the dimensionless needle size. Gul et al. [36] also contributed to the research project on CNTs nanofluids by executing a model with magnetic effect and viscous dissipation examinations. In contrast to the thickness of the boundary layers, they noticed that the thin needle reacts rapidly to a rise in heat transfer rate over the surface of the thin needle. The scientific papers by Afridi et al., Sreedevi et al., and Nayak et al. [37–39] serve as examples of how other researchers have focused on the flow of CNTs over a thin needle.

The vast amount of literature on the flow of CNTs nanofluids has focused on water as the base fluid. As for what role base fluids play, Bharat et al. [40] looked into it and came to the conclusion that they had a big effect on the thermal properties of NFs and could help make NFs better at conducting heat. This phenomenon prompted Salleh et al. [41] to evaluate various CNTs-based fluid models (water and kerosene) over

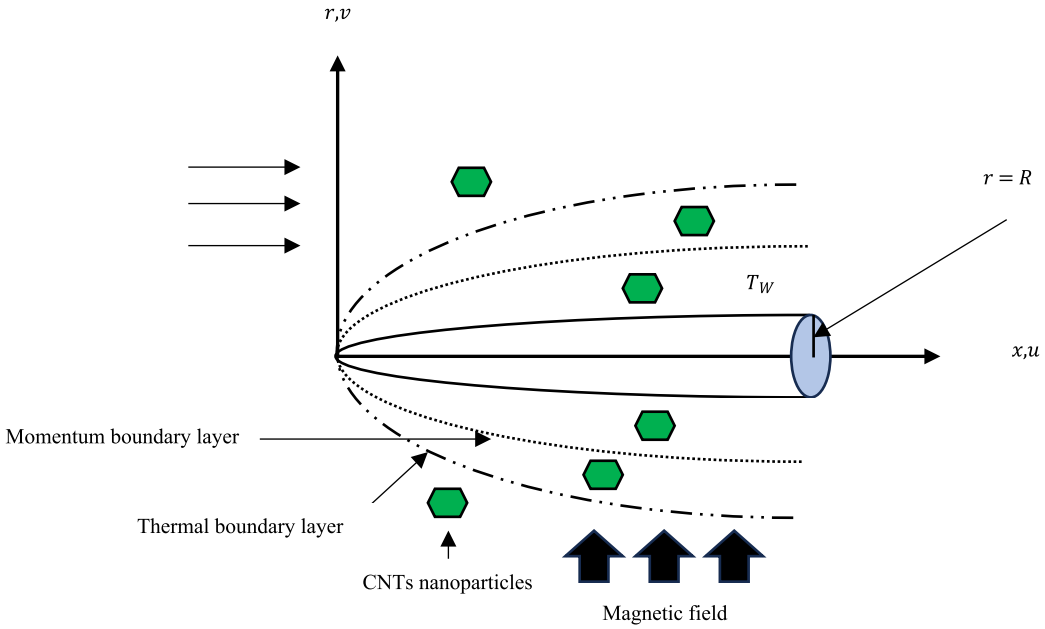

Fig. 1. Schematic model.

a moving thin needle. They discovered that kerosene-based CNTs demonstrated the highest skin friction coefficient and heat transfer rate when compared to water-based CNTs. They also demonstrated the existence of non-unique solutions by reversing the direction of the needle.

From the literature, to date, we have not yet found the exploration of CNTs nanofluids flow past a horizontal moving thin needle under the influence of magnetohydrodynamic (MHD) using different base fluids. This research has chosen CNTs as the main nanoparticle due to their excellent thermophysical properties and eco-friendly material compared to other regular nanoparticles. We also observe that CNTs have been applied below 4 % (SWCNTs: 1 % and MWCNTs: 2 %) in the area of improving thermal performance, as reported by Olia et al. [42]. The utilisation of CNTs in small applications has motivated us to further study their potential for investigating the behaviour of fluid flow and heat transfer. The challenge of picking between SWCNTs or MWCNTs to improve heat transmission on various surfaces also serves as a driving force for conducting this model. In previous studies, Anuar et al. [43] conducted research that concluded that MWCNTs were the most effective type of CNTs. In contrast, Samat et al. [44] achieved results that contradicted the findings of Anuar et al. [43]. Aziz et al. [45] found that water is the most commonly used base fluid, accounting for approximately 87 % of nanofluids preparations. However, we are looking for a substitute for the traditional fluid that incorporates CNTs. Therefore, our proposal is to utilise kerosene in combination with CNTs and conduct a numerical comparison of the performance between water and kerosene. Aziz et al. [45] discovered that the preparation of nanofluids using kerosene is on a small scale, accounting for nearly 2 %. This opportunity allows us to further explore the flow behaviour of CNTs nanofluids with kerosene and fill a research gap in this field. To explain MHD, according to Ibrahim et al. [46], we can classify it as a magnetic parameter that can increase the skin friction coefficient of the surface. Ahmad et al. [47] found that MHD is a particularly fascinating subject of investigation due to the potential impacts of magnetic fields on the boundary layer flow.

As a result of previous research on how CNTs flow over a thin needle, we are deciding to broaden the work from Salleh et al. [41] by incorporating a new effect, the MHD effect, as a result of previous research on CNTs flow over a thin needle. The current investigation differs from those by Salleh et al. [41], as they did not take into account the MHD effect on the flow when governing the model and did not perform an optimisation procedure for the heat transmission. The magnetic parameter term employed in our model is distinct from that of Gul et al.'s approach [36].

The main purpose of constructing this model is to determine the types of solutions and the expansion of their range as a result of the MHD effect. We also observe the effect of MHD on the flow behaviour within the boundary layer by evaluating the point at which the separation of the boundary layer occurred. Based on the previous models, the production of dual solutions enables researchers to precisely estimate the detachment of the boundary layer.

To generate the approximate numerical solutions, MATLAB R2022b bvp4c with a particular tolerance is coded and used. In order to meet practical requirements, the efficacy of CNTs on physical quantities is measured by computing the skin friction coefficient and the local Nusselt number. Different parameters that may influence the coefficient of skin friction and heat transmission, especially MHD effect, are analysed, and the results are represented graphically.

Response surface methodology (RSM) is used to find the best solution for important physical quantities after the numerical experiment has been run. This is the last step in our research methodology. Most research has carried out stability analysis; there is very little scientific publication on performing the optimisation approach on numerical experiments. Motivation to enhance the model's quality: Minitab is chosen as a statistical and mathematical testing instrument for the coded model after recognising several factors and their responses.

Before we begin our investigation, we outline the following objectives for this exploration:

- To develop a mathematical model for the flow of CNTs nanofluids across a moveable thin needle using two distinct based fluids (water and kerosene).
- To transform the model that consists of partial differential equations into non-dimensional ordinary differential equations using the similarity transform method.
- To identify the region where the dual solutions occur for the desired solutions.
- To create a predictive flow separation model using the dual solutions due to the various parameter modifications.
- To examine the way in which changes in the size of the thin needle and magnetic parameters affect the growth of the desired solutions.

Table 1
The thermo-physical characteristics of CNTs and the based fluids at room temperature, as studied by Nayak et al., Aladdin et al., Khan et al., and Dinarvand et al. [39,50,53,54].

Thermophysical properties	Nanoparticles		Base fluids	
	SWCNTs	MWCNTs	Water	Kerosene
Density, ρ (kg/m^3)	2600	1600	997	783
Specific heat, C_p (J/kg K)	425	796	4179	2090
Electrical conductivity, σ (S/m)	1.0×10^{8}	3.5×10^{6}	5.0×10^{-2}	5.0×10^{-11}
Thermal conductivity, k (W/m K)	6600	3000	0.613	0.145

Table 2
The thermo-physical correlations of CNTs nanofluids, as in Dinarvand et al., Dinarvand et al., Xue, Oztop et al., and Dinarvand et al. [18,54,58–60].

Properties	Correlations
Dynamic viscosity	$\mu_{nf}=\frac{\mu_f}{(1-\phi)^{2.5}}$
Density	$\rho_{nf}=(1-\phi)\rho_f+\phi\rho_{CNT}$
Heat capacity	$(\rho C_p)_{nf}=(1-\phi)(\rho C_p)_f+\phi(\rho C_P)_{CNT}$
Thermal conductivity	$k_{nf}=k_f\left(\frac{(1-\phi)+2\phi\frac{k_{CNT}}{k_{CNT}-k_f}\ln\frac{k_{CNT}+k_f}{2k_f}}{(1-\phi)+2\phi\frac{k_f}{k_{CNT}-k_f}\ln\frac{k_{CNT}+k_f}{2k_f}}\right)$
Electrical conductivity	$\sigma_{nf}=\sigma_f\left(1+\frac{3\phi\left(\frac{\sigma_{CNT}}{\sigma_f}-1\right)}{\left(\frac{\sigma_{CNT}}{\sigma_f}+2-\left(\frac{\sigma_{CNT}}{\sigma_f}-1\right)\phi\right)}\right)$

- To investigate a number of factors influencing the skin and heat transfer coefficients.
- To generate the second-order regression models using three factors.
- To maximise the heat transfer coefficient of CNTs nanofluids based on three factors using RSM.

2. Mathematical formulation

To construct this model, we referenced a number of sources from Yasir et al., Salleh et al., Salleh et al., and Aladdin et al. [29,48–50]. In order to clarify the physical model as illustrated in Fig. 1, we establish the following assumptions:

- The formulation of the model is based on Tiwari and Das's model.
- This model covers two-dimensional (2D)x and r coordinate orientations.
- We set r, where r symbolizes the radial coordinates in cylindrical form and perpendicular to the thin surface.
- The thin needle is assumed to be immersed in two different CNTs nanofluids: CNTs nanofluids/water and CNTs nanofluids/kerosene.
- The flow of CNTs nanofluids is characterized by steady, incompressible, and laminar flows.
- The movable thin needle across the fluid motion under the MHD effect.
- By following the previous study from Mabood et al. [51], the thickness of the thin needle is adjusted to be smaller than that of the thermal and momentum boundary layers over it.
- Two horizontal dimensions of the movement of the thin needle are either portrayed in the same direction ($\lambda>0$) or in the opposite direction ($\lambda<0$).
- This paraboloid needle is also surrounded by a constant temperature, T_w and a constant ambient temperature, T_∞, where $T_\infty<T_w$.
- The movement of this needle is at composite velocity, $U=U_\infty+U_w$ as stated in Khan et al. [52], where U_w and U_∞ are velocity constants.
- The heat is transferred through free convection.
- The thermal properties of the chosen CNTs and the base fluids are depicted in Table 1.

We modify the works of Salleh et al. [41] and Salleh et al. [49] by inserting the MHD term into the momentum equation. To keep novelty of the work, we customise the MHD term introduced previously by Salleh et al., Alahmadi et al., and Asshaari et al. [48,55,56]. Hence, we develop a mathematical formulation that is compatible with our model as follows:

$$\frac{\partial}{\partial x}(ru)+\frac{\partial}{\partial r}(rv)=0 \tag{1}$$

$$u\frac{\partial u}{\partial x}+v\frac{\partial u}{\partial r}=\frac{\mu_{nf}}{\rho_{nf}}\frac{1}{r}\frac{\partial}{\partial r}\left(r\frac{\partial u}{\partial r}\right)+\frac{\sigma_{nf}}{\rho_{nf}}B^2(U-u), \tag{2}$$

$$u\frac{\partial T}{\partial x}+v\frac{\partial T}{\partial r}=\frac{\alpha_{nf}}{r}\frac{\partial}{\partial r}\left(r\frac{\partial T}{\partial r}\right). \tag{3}$$

The complete boundary conditions are written as follows:

$$\begin{aligned} &u=U_w,\ v=0,\ T=T_w \text{ at } r=R(x),\\ &u\to U_\infty,\ T\to T_\infty \text{ as } r\to\infty. \end{aligned} \tag{4}$$

The velocity elements are defined by u and v, which move along the (x,r) directions. The$x-$axis is determined along the surface and the$r-$radial axis was normal to the$x-$axis. The term of μ_{nf}/ρ_{nf} are written as $\nu_{nf}=\mu_{nf}/\rho_{nf}$, where ν_{nf} is the effective kinematic viscosity. The constant B is the magnetic field, as in Samat et al. [57], applied to the fluid flow such that $B=B_0\sqrt{x}$. The thermal correlations of CNTs nanofluids are depicted in Table 2.

In an effort to decrease the complexity of the computation procedures, the nonlinear partial differential equations (PDEs) in Eqs. (2) – (3), are transformed into non-dimensional ordinary equations (ODEs). In the conversion procedure, we utilise the following similarity variables proposed by Salleh et al. [41] and Aladdin et al. [61]:

$$\eta=\frac{Ur^2}{\nu_f x},\psi=\nu_f x f(\eta),r=R(x)=\sqrt{\frac{\nu_f\eta x}{U}},\theta(\eta)=\frac{T-T_\infty}{T_w-T_\infty}, \tag{5}$$

where ψ represents the dimensionless stream function depending on η. The transformation of u and v, which reflect the velocity components in 2D to dimensionless components are expressed in the following forms:

$$u=\frac{1}{r}\frac{\partial\psi}{\partial r},v=-\frac{1}{r}\frac{\partial\psi}{\partial x}. \tag{6}$$

Implementing the similarity variables as expressed in Eq. (5), PDEs in Eqs. (2) – (3) are transformed into ODEs of the following forms:

$$2\frac{A_1}{A_2}(\eta f'''+f'')+ff''+\frac{A_3}{A_2}M(1-2f')=0, \tag{7}$$

$$\frac{2}{\mathrm{Pr}}\frac{A_4}{A_5}(\eta\theta''+\theta')+f\theta'=0, \tag{8}$$

where the function of f depends on η. With respect to η, the derivatives of f''',f'',f',θ'', and θ' are also computed. The term M can be denoted as $M=\frac{\sigma_f}{\rho_f}\frac{B_0^2}{2U}$ (Yasir et al. [29]). The following expressions can be used for composing the terms A_i, $i=1,2,\cdots,5$:

$$A_1=\frac{\mu_{nf}}{\mu_f},A_2=\frac{\rho_{nf}}{\rho_f},A_3=\frac{\sigma_{nf}}{\sigma_f},A_4=\frac{k_{nf}}{k_f},A_5=\frac{(\rho C_p)_{nf}}{(\rho C_p)_f} \tag{9}$$

Eqs. (7) – (9) are subjected to the transformation boundary conditions as follows:

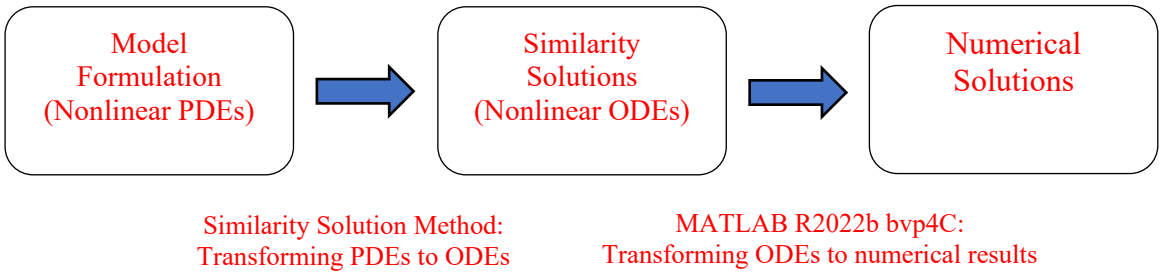

Fig. 2. Computational approaches to the model.

Table 3
The matrix of significant parameters into the coded symbols.

Parameters	Coded Symbols
ϕ	x_1
M	x_2
c	x_3

Table 4
The validation with previous works.

The size of needle,c	Ali et al. [4]	Salleh et al. [41]	Waini et al. [71]	Present Study
The size of needle,c	Ali et al. [4]	Salleh et al. [41]	Waini et al. [71]	Present Study
0.01	26.59396	26.599394	26.599394	26.599394
0.05	–	–	–	6.726245
0.10	3.70711	3.703713	3.703714	3.703713
0.20	2.005421	2.005424	2.005427	2.005424
0.25	–	–	–	1.634343
0.30	–	–	1.377147	1.377142
0.40	–	–	–	1.040475
0.01	26.59396	26.599394	26.599394	26.599394
0.05	–	–	–	6.726245
0.10	3.70711	3.703713	3.703714	3.703713
0.20	2.005421	2.005424	2.005427	2.005424
0.25	–	–	–	1.634343
0.30	–	–	1.377147	1.377142
0.40	–	–	–	1.040475

$$f'(\eta)=\frac{\lambda}{2}, f(\eta)=\frac{\lambda}{2}c,\ \theta(\eta)=1 \text{ at } \eta=c,$$
$$f'(\eta)=-\left(\frac{\lambda-1}{2}\right),\ \theta(\eta)=0 \text{ as } \eta\to\infty, \tag{10}$$

where c is the dimensionless needle size.

Next, we set up the skin friction coefficient, C_f, and the local Nusselt number, Nu_x, as follows, since one of our primary objectives is to examine how different parameters influence the efficiency of heat transmission:

$$C_f=\frac{\tau_w}{\rho_f U^2}, Nu_x=\frac{xq_w}{k_f(T_w-T_\infty)}, \tag{11}$$

where τ_w and q_w are the surface shear stress and the heat flux, respectively. The terms τ_w and Nu_x can be expressed as

$$\tau_w=\mu_{nf}/\mu_f\left(\frac{\partial u}{\partial r}\right) at\ r=c,$$
$$q_w=-k_{nf}/k_f\left(\frac{\partial T}{\partial r}\right) \text{at } r=c \tag{12}$$

To complete the forms of τ_w and q_w in Eq. (12), the terms T from Eq. (5) and u from Eq. (6) are differentiated with respect to r. The results from these differentiations are substituted into Eq. (12). After some rearranging of Eq. (12), hence, Eq. (12) becomes

$$C_f(Re_x)^{1/2}=\frac{4}{(1-\phi)^{2.5}}(c)^{1/2}f''(c),$$
$$Nu_x(Re_x)^{-1/2}=-2\frac{k_{nf}}{k_f}(c)^{1/2}\theta'(c), \tag{13}$$

where $Re_x=U_x/\nu_x$ represents the local Reynolds numbers. According to Roy et al. [62], the Nusselt number is a crucial factor that can enhance

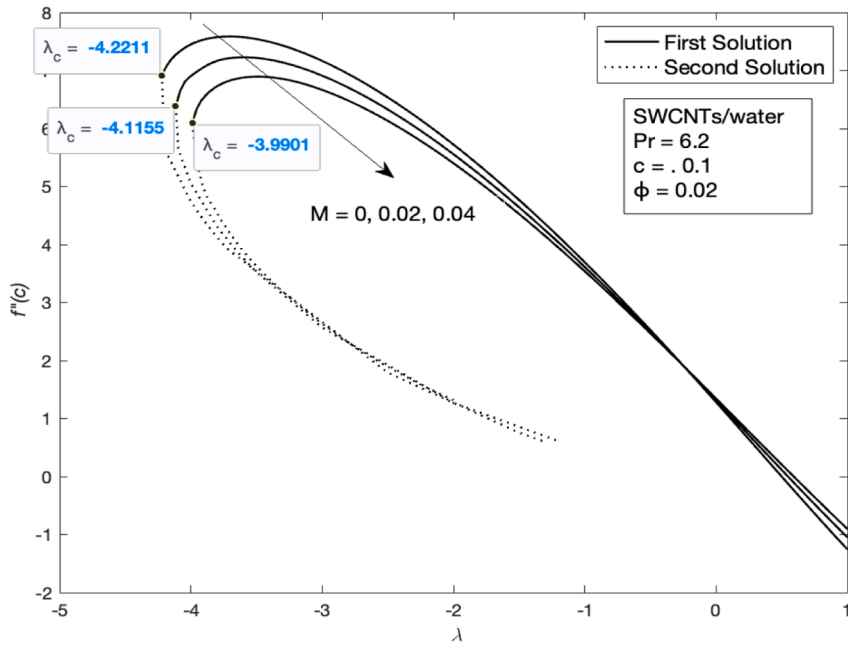

(a)

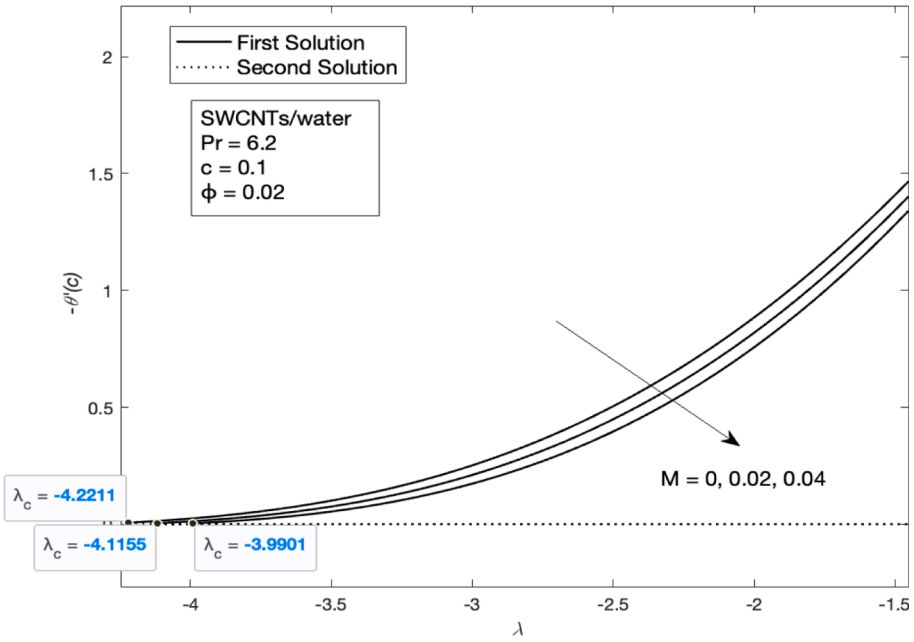

(b)

Fig. 3. Variation of (a) $f^{'}(c)$ and (b) $-\theta'(c)$ with different M and λ for SWCNTs/water.

the rate of heat transfer.

3. Method of solution and code validation

To be able to solve the model, we implement two parts of the computational strategies, as depicted in Fig. 2. Part I involves numerical procedures using the bvp4c programme in MATLAB R2022b. To optimise the heat transfer rate, in Part II, we utilise response surface methodology (RSM) by using three parameters. The parameters are selected based on the effects emphasised by Eqs. (7) – (10) and Tiwari and Das's model, specifically the volume fraction of CNTs, ϕ.

3.1. Numerical scheme

The similarity solutions (Eqs. (7) – (10)) that are produced for this model deal with a higher-order ODEs system. In order to solve the

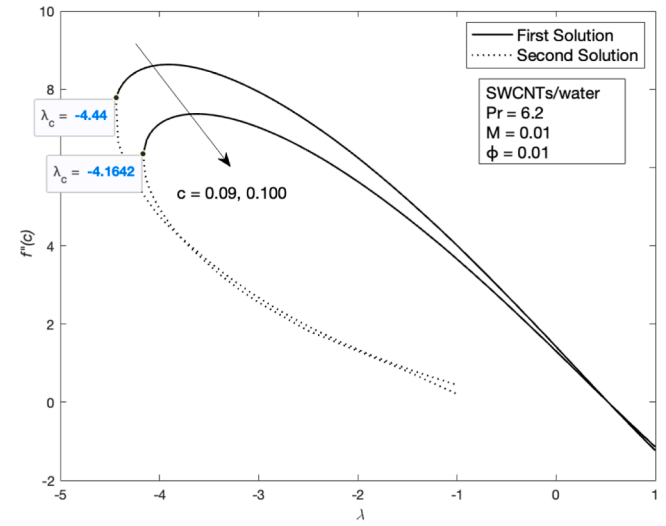

(a)

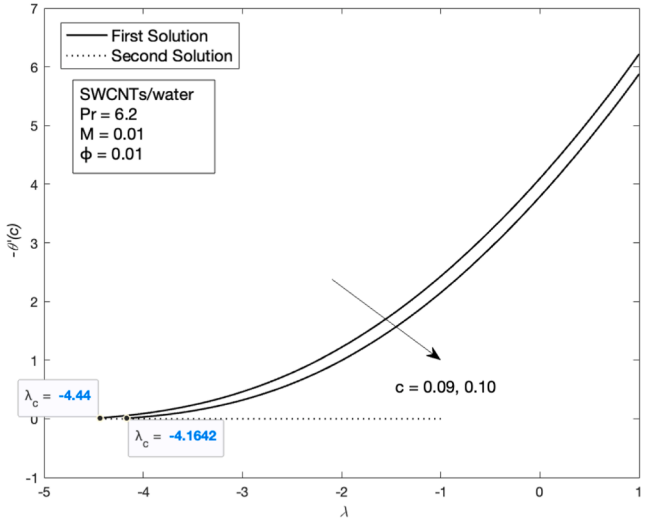

(b)

Fig. 4. Variation of (a) $f'(c)$ and (b) $-\theta'(c)$ with different c and λ for SWCNTs/water.

nonlinear ODEs system numerically, Abbas et al. [63] stated that the higher-order ODEs required being converted into first-order ODEs. Hence, the nonlinear higher-order ODEs system expressed in Eqs. (7) – (10) are converted to nonlinear first-order ODEs before operating the codes numerically. The first-order ODEs are structured in the expressions below:

$$f(\eta) = y(1), f'(\eta) = y(2), f''(\eta) = y(3), \theta(\eta) = y(4), \theta'(\eta) = y(5), f''(\eta) = -\frac{1}{\eta}\left[y(3) + \frac{1}{2}\frac{A_2}{A_1}\left(y(1)y(3) + \frac{A_3}{A_2}M(1-2y(2)\right)\right] \quad (14)$$
$$\theta''(\eta) = -\frac{1}{\eta}\left[y(5) + \frac{\mathrm{Pr}}{2}\frac{A_5}{A_4}(y(1)y(5))\right]$$

The boundary conditions in first-order ODEs are written as

$$ya(1) - \frac{\lambda}{2}c = 0,\ ya(2) - \frac{\lambda}{2} = 0, ya(4) - 1 = 0,$$
$$yb(2) + \left(\frac{\lambda - 1}{2}\right) = 0, yb(4) = 0, \quad (15)$$

where a describes $\eta = c$ and b defines $\eta \to \infty$. The bvp4c function built into MATLAB can be used to compute the first order in Eq. (14) and the boundary conditions in Eq. (15). Khan et al. [64] believed that the bvp4c function, utilising a finite difference method, is one of the finest ways to solve first-order ODEs. This package has also applied an adaptive mesh solver to solve the ODEs model. Ali [65] also noticed that it can provide a platform that is efficient in terms of computational processes. We anticipate that the numerical solutions, under specific parameters, will produce two solutions: an upper branch and a lower branch. To generate them, we construct the codes using varying initial guess values to satisfy the boundary criteria in Equation (15). Because the initial guess values for the lower solution (second solution) are harder to guess compared to the upper solution (first solution), we organised the continuing codes to estimate the set of solutions. To set up the maximum η, which symbolises $\eta \to \infty$, we select η up to 60 depending on the control values of the parameters. To attain the convergence criterion of the velocity and temperature profiles, the iterated computing procedure is performed at tolerance limit 10^{-6}.

3.2. Optimisation procedure using RSM

During the development of the model and execution of the numerical experiment, several significant independent variables, often referred to as factors, have an impact on the physical quantities, also known as responses. The analysis of the relationship between variables and their responses may be conducted using several optimisation programs, including RSM. According to Lamidi et al. [66], RSM is widely recognised as an excellent experimental design technique. This is because it facilitates the fabrication of a highly robust design of experiments (DOE) instrument, which is crucial in generating optimisation outcomes. The success of RSM may be attributed to its capacity to effectively use mathematical and statistical techniques in analysing the correlation between various factors and corresponding outcomes.

The application of RSM can accomplish the objective of maximising the heat transfer process by investigating the local Nusselt number resulting from the use of distinct factors. The adoption of RSM can effectively achieve the objective of optimising the heat transfer process by examining the local Nusselt number obtained from the implementation of various influential factors.

This model is fitted using a second-order response surface model, as this model has the potential to produce optimal solutions from the curvature surface. The expression for the second-order polynomial regression equation, which includes three controllable variables that maximise the response, $Res = y(x_1, x_2, x_3) = Nu_x Re_x^{-1/2}$ can be structurally formulated as follows:

$$Res = b_0 + b_1x_1 + b_2x_2 + b_3x_3 + b_{12}x_1x_2 + b_{13}x_1x_3 + b_{23}x_2x_3 + b_{11}x_1^2 + b_{22}x_2^2 + b_{33}x_3^2 + \epsilon, \quad (16)$$

where Res, x_1, x_2, x_3, and ϵ denote the response (outcome), the first factor, the second factor, the third factor, and the error term, respectively. The term b_0 is the overall mean response, and the regression model coefficients are represented by b_1, b_2, b_3, b_{11}, b_{12}, b_{13}, b_{22}, b_{23}, and b_{33}.

The three key components that have a potential impact on the performance of heat transmission are the CNTs nanoparticle volume fraction, ϕ denoted as 'x_1', the magnetic parameters, M marked as 'x_2', and the needle size, c labelled as 'x_3'. The matrix of three filtered parameters into the coded characters is illustrated in Table 3. The selection of these

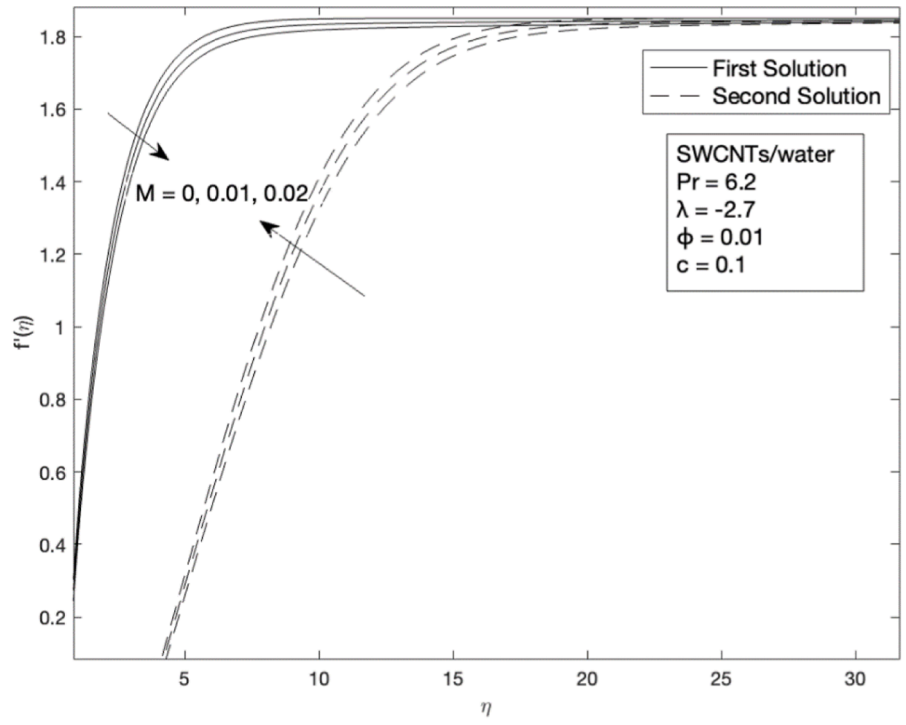

(a)

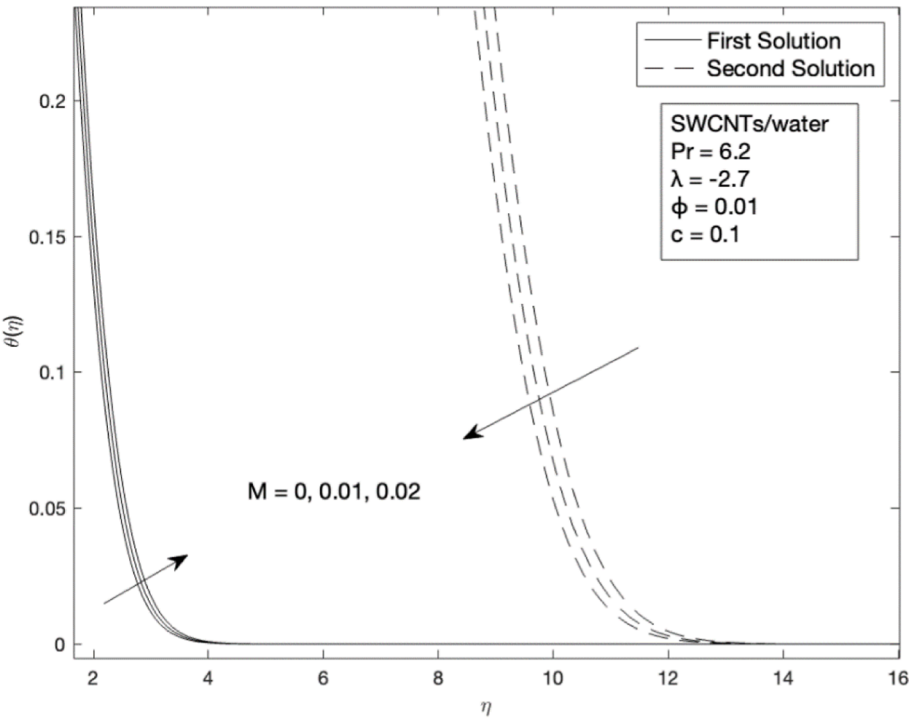

(b)

Fig. 5. Effect of different values of M on the (a) velocity and (b) temperature profiles using various η and for SWCNTs/water.

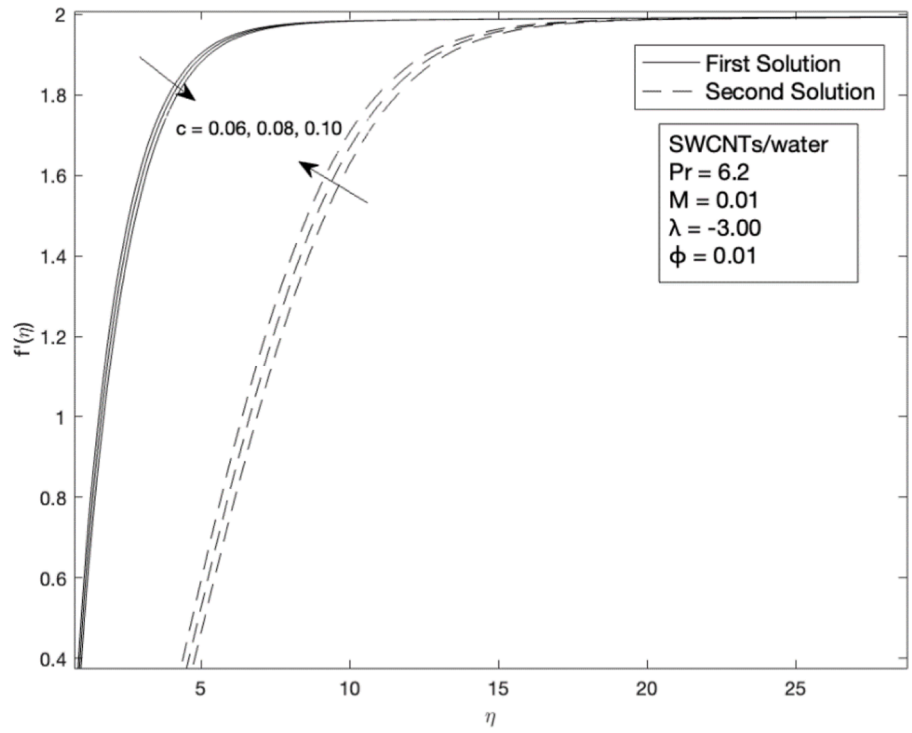

(a)

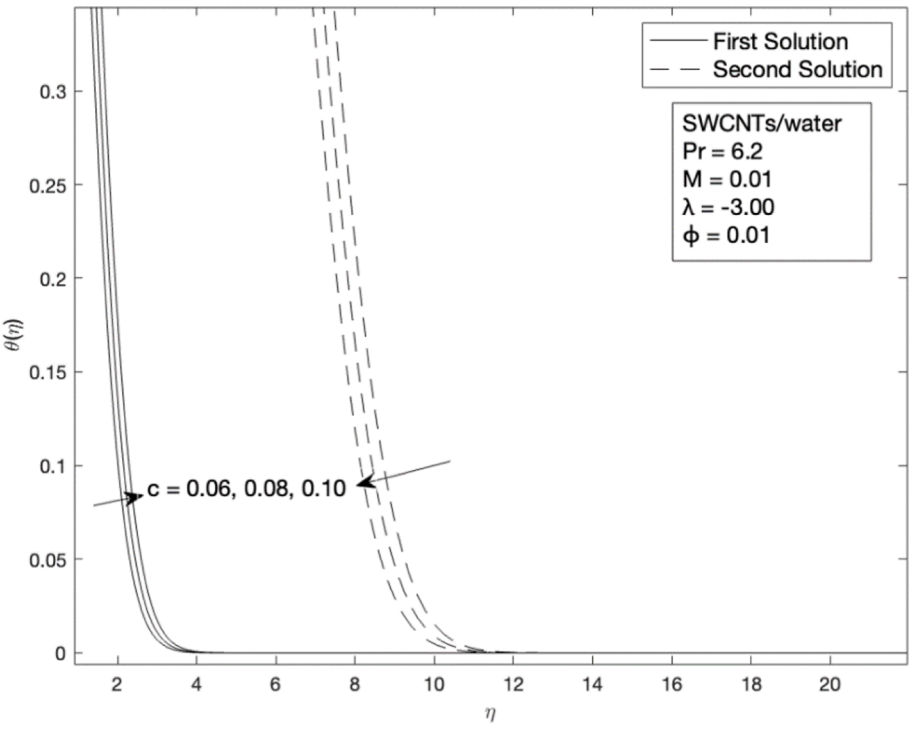

(b)

Fig. 6. Effect of different values of c on the (a) velocity and (b) temperature profiles using various η and for SWCNTs/water.

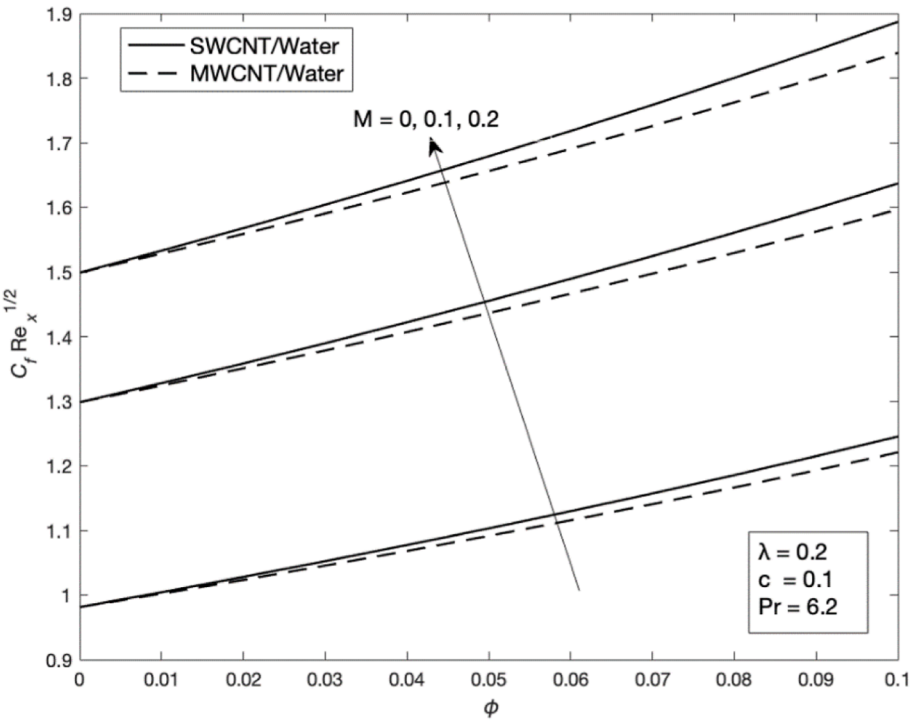

(a)

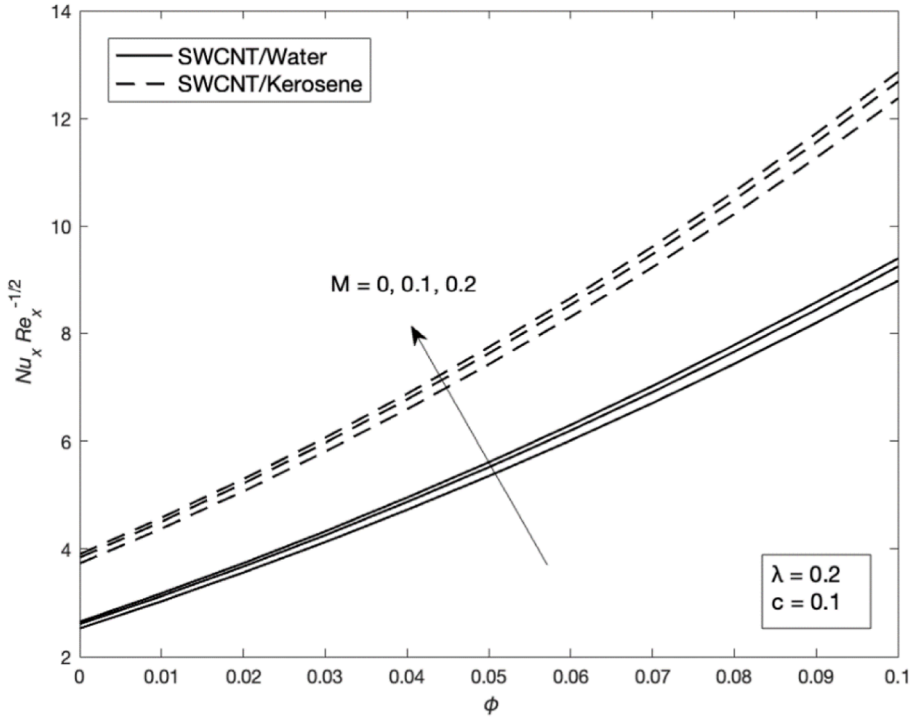

(b)

Fig. 7. Influence of different values of M on the (a) local skin friction and (b) heat transfer coefficients using various ϕ for SWCNTs/water and SWCNTs/kerosene.

independent components is based on the most significant parameter in Tiwari and Das's model, which is ϕ, as well as on Eqs. (7) – (10), which represent the variables M and c.

The first factor, denoted as x_1, can potentially be used to characterise the impact of the nanoparticle volume fraction in either SWCNTs nanoparticles or MWCNTs nanoparticles. So, the experimental designs are based on two different responses, Res_A and Res_B, which are the heat transfer responses for SWCNTs and MWCNTs, respectively. Res_A and Res_B can be illustrated as

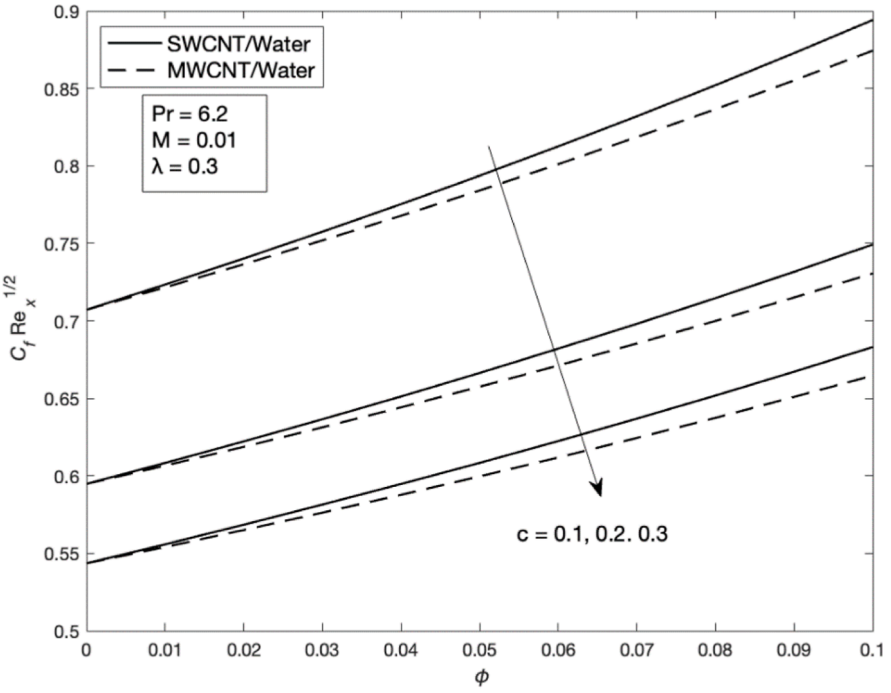

(a)

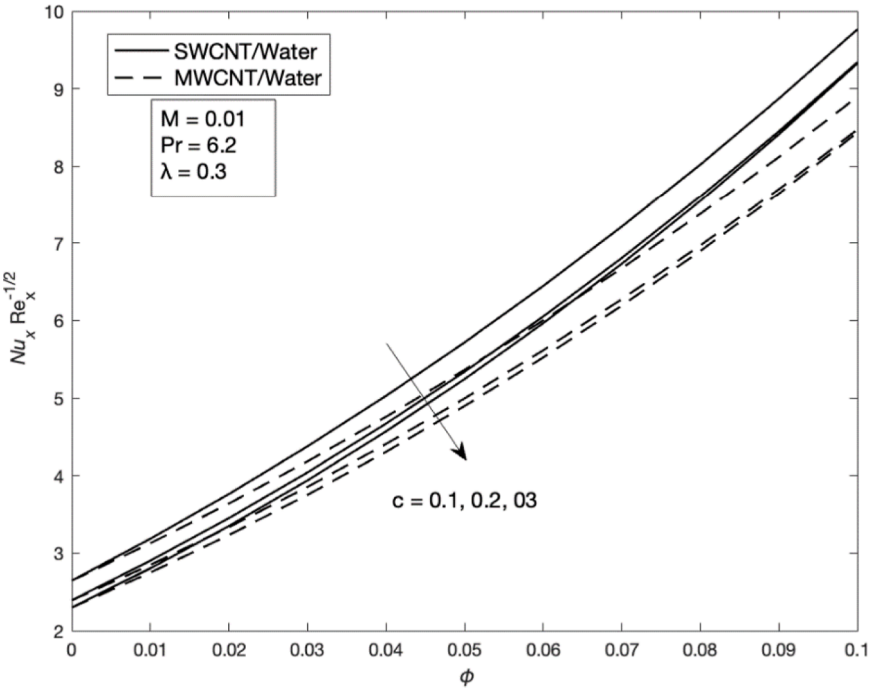

(b)

Fig. 8. Influence of different values of c on the (a) local skin friction and (b) heat transfer coefficients using various ϕ for SWCNTs/water and MWCNTs/water.

Table 5
Arrangement of coded symbols and uncoded parameters in three categories.

Parameters	Coded Symbols	Levels		
		High[+ 1]	Medium [0]	Low[−1]
ϕ	x_1	0.03	0.02	0.01
M	x_2	0.3	0.2	0.1
c	x_3	0.3	0.2	0.1

Table 6
Variation settings for coded symbols and uncoded parameters and responses for SWCNTs and MWCNTs.

Trials	Coded Symbols			Uncoded Parameters			Responses	
	x_1	x_2	x_3	ϕ	M	c	Res_A	Res_B
1	−1	−1	−1	0.01	0.1	0.1	3.2861	3.2260
2	1	−1	−1	0.03	0.1	0.1	4.5112	4.3111
3	−1	1	−1	0.01	0.3	0.1	3.3810	3.3191
4	1	1	−1	0.03	0.3	0.1	4.6391	4.4334
5	−1	−1	1	0.01	0.1	0.3	2.8918	2.8354
6	1	−1	1	0.03	0.1	0.3	4.0551	3.8629
7	−1	1	1	0.01	0.3	0.3	2.9789	2.9208
8	1	1	1	0.03	0.3	0.3	4.1723	3.9748
9	−1	0	0	0.01	0.2	0.2	3.0500	2.9920
10	1	0	0	0.03	0.2	0.2	4.2377	4.0421
11	0	−1	0	0.02	0.1	0.2	3.5594	3.4383
12	0	1	0	0.02	0.3	0.2	3.6643	3.5398
13	0	0	−1	0.02	0.2	0.1	3.9483	3.8192
14	0	0	1	0.02	0.2	0.3	3.5141	3.3915
15	0	0	0	0.02	0.2	0.2	3.6236	3.5004
16	0	0	0	0.02	0.2	0.2	3.6236	3.5004
17	0	0	0	0.02	0.2	0.2	3.6236	3.5004
18	0	0	0	0.02	0.2	0.2	3.6236	3.5004
19	0	0	0	0.02	0.2	0.2	3.6236	3.5004
20	0	0	0	0.02	0.2	0.2	3.6236	3.5004

Table 7
ANOVA for the heat transfer coefficient using SWCNTs.

Source	DF	Adj SS	Adj MS	*F*-Value	*P*-Value
Model	9	4.25970	0.47330	7423.42	0.000
Linear	3	4.18693	1.39564	21889.76	0.000
x_1	1	3.68158	3.68158	57743.19	0.000
x_2	1	0.02421	0.02421	379.66	0.000
x_3	1	0.48114	0.48114	7546.44	0.000
Square	3	0.06919	0.02306	361.72	0.000
$x_1 \times x_1$	1	0.00133	0.00133	20.82	0.001
$x_2 \times x_2$	1	0.00028	0.00028	4.34	0.064
$x_3 \times x_3$	1	0.03287	0.03287	515.49	0.000
2-Way Interaction	3	0.00359	0.00120	18.77	0.000
$x_1 \times x_2$	1	0.00007	0.00007	1.05	0.330
$x_1 \times x_3$	1	0.00347	0.00347	54.35	0.000
$x_2 \times x_3$	1	0.00006	0.00006	0.91	0.364
Error	10	0.00064	0.00006		
Lack-of-Fit	5	0.00064	0.00013	*	*
Pure Error	5	0.00000	0.00000		
Total	19	4.26034			

$$Res_A = y_{SWCNT}(x_1, x_2, x_3) = \left(Nu_x Re_x^{-\frac{1}{2}} \right)_{SWCNT}, \tag{17}$$

$$Res_B = y_{MWCNT}(x_1, x_2, x_3) = \left(Nu_x Re_x^{-\frac{1}{2}} \right)_{MWCNT}. \tag{18}$$

The evaluation of heat transfer performance between SWCNTs and MWCNTs can be determined by analysing the Res_A and Res_B outcomes.

In order to construct a design matrix that adheres to established requirements, it is necessary to precisely determine the number of trials, N. As the design involves two levels of design, the term N can be computed by using the formula below:

$$N = 2^F + 2F + C, \tag{19}$$

where F stands for the number of factors and C belongs to the centre points.

We use the approach that several studies, including Mahanthesh et al., Jawairia et al., and Yahaya et al. [67–69], have used to construct

Table 8
ANOVA for the heat transfer coefficient using MWCNTs.

Source	DF	Adj SS	Adj MS	*F*-Value	*P*-Value
Model	9	3.38056	0.37562	22126.47	0.000
Linear	3	3.31928	1.10643	65176.03	0.000
x_1	1	2.84196	2.84196	167410.52	0.000
x_2	1	0.02644	0.02644	1557.51	0.000
x_3	1	0.45088	0.45088	26560.06	0.000
Square	3	0.05912	0.01971	1160.84	0.000
$x_1 \times x_1$	1	0.00076	0.00076	44.49	0.000
$x_2 \times x_2$	1	0.00036	0.00036	21.15	0.001
$x_3 \times x_3$	1	0.03025	0.03025	1781.65	0.000
2-Way Interaction	3	0.00217	0.00072	42.54	0.000
$x_1 \times x_2$	1	0.00039	0.00039	22.84	0.001
$x_1 \times x_3$	1	0.00174	0.00174	102.35	0.000
$x_2 \times x_3$	1	0.00004	0.00004	2.41	0.151
Error	10	0.00017	0.00002		
Lack-of-Fit	5	0.00017	0.00003	*	*
Pure Error	5	0.00000	0.00000		
Total	19	3.38073			

Table 9
The reduced model of the heat transfer coefficient using SWCNTs.

Source	DF	Adj SS	Adj MS	*F*-Value	*P*-Value
Model	6	4.25930	0.70988	8885.83	0.000
Linear	3	4.18693	1.39564	17469.68	0.000
x_1	1	3.68158	3.68158	46083.42	0.000
x_2	1	0.02421	0.02421	303.00	0.000
x_3	1	0.48114	0.48114	6022.63	0.000
Square	2	0.06891	0.03446	431.29	0.000
$x_1 \times x_1$	1	0.00106	0.00106	13.29	0.003
$x_3 \times x_3$	1	0.03566	0.03566	446.35	0.000
2-Way Interaction	1	0.00347	0.00347	43.38	0.000
$x_1 \times x_3$	1	0.00347	0.00347	43.38	0.000
Error	13	0.00104	0.00008		
Lack-of-Fit	8	0.00104	0.00013	*	*
Pure Error	5	0.00000	0.00000		
Total	19	4.26034			

Table 10
The reduced model of the heat transfer coefficient using MWCNTs.

Source	DF	Adj SS	Adj MS	*F*-Value	*P*-Value
Model	8	3.38052	0.42257	2,205,970	0.000
Linear	3	3.31928	1.10643	55760.12	0.000
x_1	1	2.84196	2.84196	148362.09	0.000
x_2	1	0.02644	0.02644	1380.29	0.000
x_3	1	0.45088	0.45088	23537.98	0.000
Square	3	0.05912	0.01971	1028.75	0.000
$x_1 \times x_1$	1	0.00076	0.00076	39.43	0.000
$x_2 \times x_2$	1	0.00035	0.00036	18.75	0.001
$x_3 \times x_3$	1	0.03025	0.03025	1578.93	0.000
2-Way Interaction	2	0.00213	0.00106	55.48	0.000
$x_1 \times x_2$	1	0.00039	0.00039	20.25	0.001
$x_1 \times x_3$	1	0.00174	0.00174	90.71	0.000
Error	11	0.00021	0.00002		
Lack-of-Fit	6	0.00021	0.00004	*	*
Pure Error	5	0.00000	0.00000		
Total	19	3.38073			

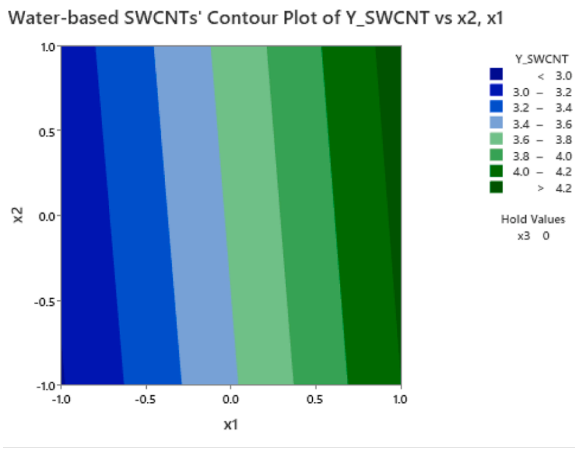

(a)

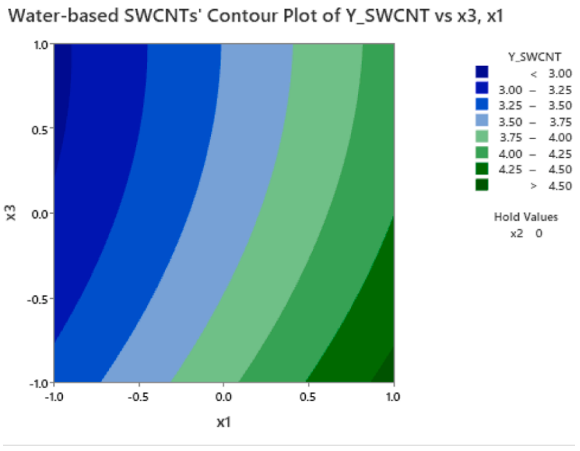

(b)

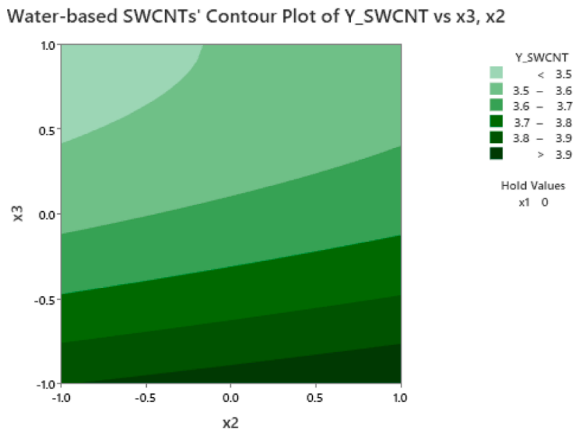

(c)

Fig. 9. Contour (a) – (c) plots of the heat transfer using SWCNTs/water for various interactions between parameters.

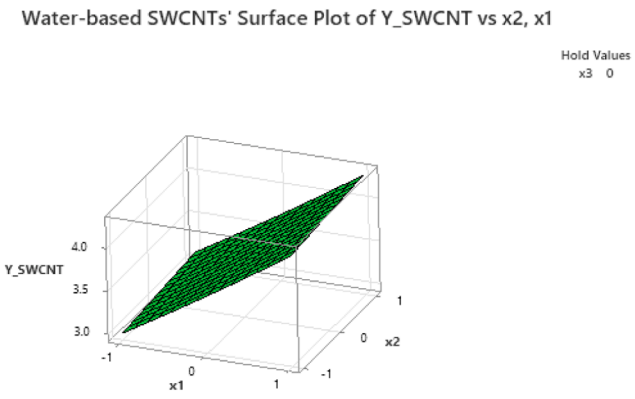

(a)

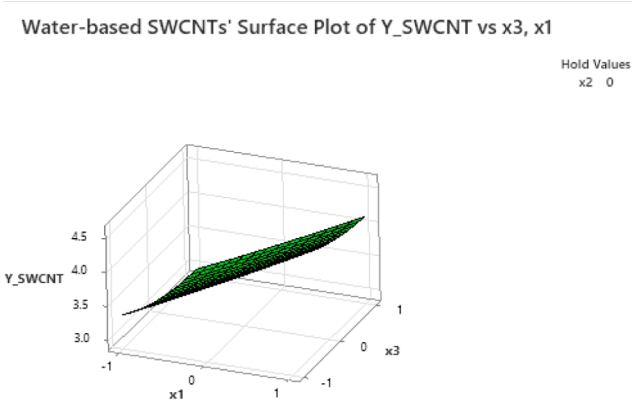

(b)

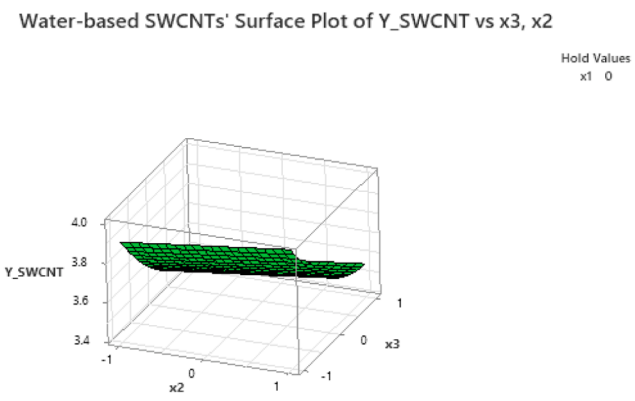

(c)

Fig. 10. Surface (a) – (c) plots of the heat transfer using SWCNTs/water for various interactions between parameters.

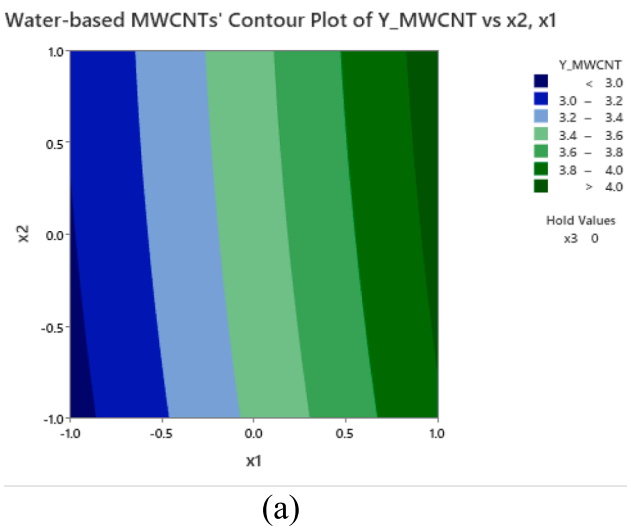

(a)

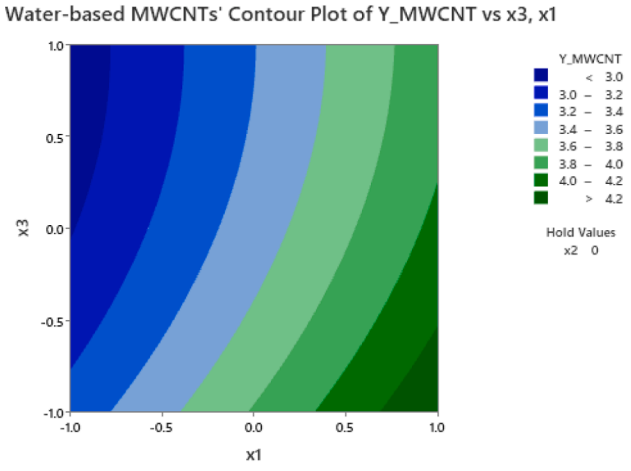

(b)

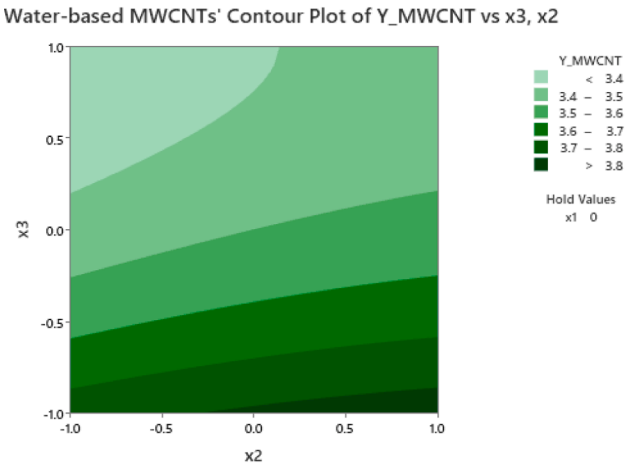

(c)

Fig. 11. Contour (a) – (c) plots of the heat transfer using MWCNTs/water for various interactions between parameters.

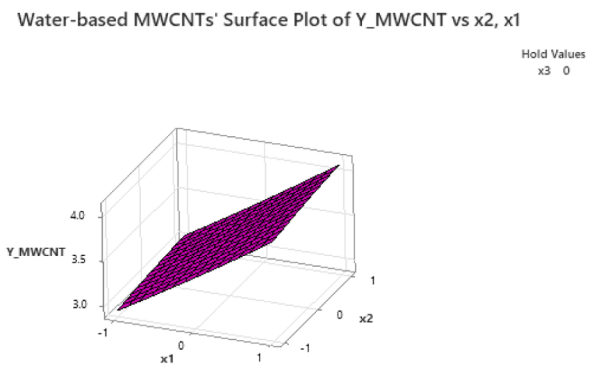

(a)

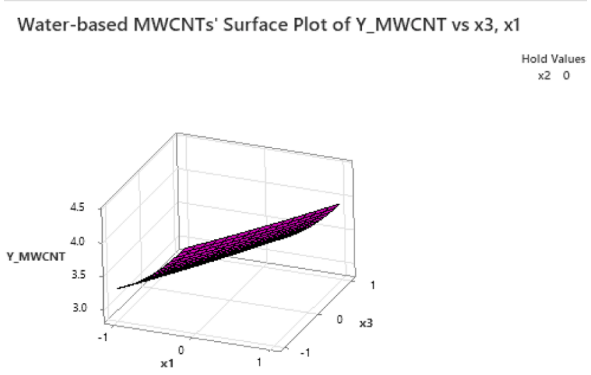

(b)

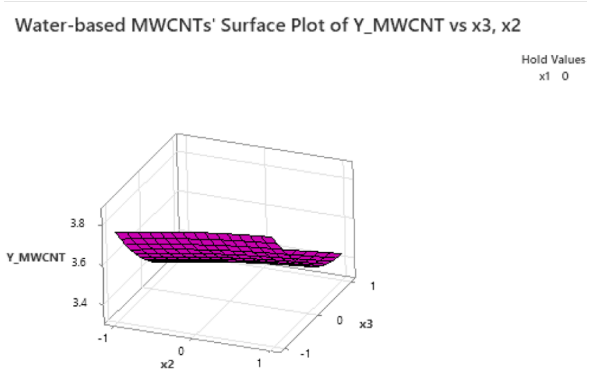

(c)

Fig. 12. Surface (a) – (c) plots of the heat transfer using MWCNTs/water for various interactions between parameters.

Table 11
Response optimisation solution for the heat transfer rate using SWCNTs.

Response	Solution			y_{SWCNT}Fit	CompositeDesirability
	x_1	x_2	x_3		
y_{SWCNT}	1	1	−1	4.64155	1

Table 12
Response optimisation solution for the heat transfer rate using MWCNTs.

Response	Solution			y_{MWCNT}Fit	CompositeDesirability
	x_1	x_2	x_3		
y_{MWCNT}	1	1	−1	4.42901	0.997252

the experimental design. They performed RSM adopting the face-centred central composite design (CCF). This design generally involves setting the value of A $= 1$, where A represents the distance between the star points and the centre. To modify the original numeric values into the coded values, we assign the coded values of $+1$, 0, and -1 to represent the largest, middle, and smallest values of the factors, respectively. This enables us to incorporate the responses into the matrix, which displays the data in a coded format.

The validation of the design is conducted using the analysis of variance (ANOVA) technique. The results of the *P*-value test, which adhere to the generally accepted limit of 0.05 or below, demonstrate that the model has statistical significance in accordance with the findings of Samat et al. [70]. Finally, the optimising step is executed using the response optimiser. Optimal outcomes of responses are deemed acceptable when the desired function value reaches a level close to 1 or 100%.

3.3. Testing for code validation

To assure the precision and uniformity of our programming codes, we conduct tests by comparing them with multiple models that focus on the flow of boundary layer nanofluids across slim needles. The previous models by Ali et al., Salleh et al., and Waini et al. [4,41,71] serve as the foundation for the validity of the numerical calculation. We employ the similar parameter values of $M = 0, \lambda = -1, \phi = 0$, and Pr $= 1$, which were examined by Ali et al., Salleh et al., and Waini et al. [4,41,71] in order to generate the reduced skin friction, $f''(c)$. However, we expand the range of values for c beyond Ali et al., Salleh et al., and Waini et al. [4,41,71]. The values of c at 0.05, 0.25, and 0.40 were previously selected by Singh et al. and Ibrar et al. [35,72]. These values of c have potential for future reference for code validation. The comparable $f''(c)$ values are illustrated in Table 4. The results of $f''(c)$ give us a high degree of confidence in the accuracy of our codes. This motivation has led us to continue our analysis of finding the required solutions.

4. Results and discussion

This section presents the numerical and optimisation solutions obtained using the bvp4c function in MATLAB and the RSM approach, respectively. In accordance with Eqs. (7) − (10), the parameters M, c, and λ are designated as the primary parameters in this model. The range of M is defined inside the domain $0 \leq M \leq 0.2$, which was determined by Aladdin et al., Sharma et al., and Rehman et al. [50,73,74]. When determining the values of c, we follow the range defined by Ali et al., Salleh et al., and Waini et al. [4,41,71] in their reputable studies. To classify the area of λ, we refer to Salleh et al. [41]. The values of λ that correspond to the movement of the thin needle are set towards two distinct flows: the same direction flow ($\lambda > 0$) and the opposite direction flow ($\lambda < 0$). Since the model is based on Tiwari and Das's model, we also take into account the effect of ϕ on the analysis of fluid flow and heat transfer characteristics. Kumar et al. [33] discovered that the values of ϕ were applied at low concentrations in nanofluids. By following the established values of ϕ recommended by Zhou et al. [75], the variable ϕ varies from $\phi = 0$ to $\phi = 0.1$. For the purpose of presenting the outcomes, we employ both graphical and tabular approaches.

4.1. The reduced skin friction, $f''(c)$, and heat transfer $-\theta'(c)$

The evaluation of the solutions for $f''(c)$ and $-\theta'(c)$ in response to the change in , c, and λ is shown in Fig. 3, Fig. 4, respectively. By referring to the previous studies carried out on the magnetic effects by Sharma et al. and Rehman et al. [73,74], it is possible to develop Fig. 3 with a satisfactory range of the variable M. The value of M varies from 0 to 0.04. We consider the M value less than 0.1 in order to potentially generate a coupled solution for $f''(c)$ and $-\theta'(c)$ as recommended by Aladdin et al. [50]. The parameters c, Pr, and ϕ are assigned a fixed value of 0.1, 6.2 (representing water), and 0.02, respectively. We combine SWCNTs and water for producing SWCNTs/water nanofluids. The arrangement of all the values mentioned above generates two distinct branches, namely the upper (solid line) and lower (dot line) branches for $f''(c)$ and $-\theta'(c)$, in the specific region λ. The duality solutions are actively created when $\lambda < -1$ until $f''(c)$ and $-\theta'(c)$ reach λ_c, where λ_c can be denoted as the critical value of λ. However, $f''(c)$ and $-\theta'(c)$ produce only one solution (the first solution) if the thin needle passes in the same direction ($\lambda > 0$). Based on Salleh et al.'s model [41], the first solution is considered stable and potentially accepted for physical applications and operated for optimisation. However, they found that the second solution is unstable.

The generation of dual solutions is crucial for properly foreseeing the occurrence of boundary layer separation. Estimating flow separation through experimentation is challenging. A lot of the equipment used in engineering processes requires a longer duration in the laminar phase in order to stabilise fluid motion. Therefore, we utilise a numerical method to determine the separation point by examining its variation in response to changes in M. From Fig. 3, the increase in the M from 0 to 0.04 on the flow results in a reduction in the range of solutions for $f''(c)$ and $-\theta'(c)$ and also speeds up the separation of the boundary layer. This event is similar to what Kraszewska et al. [76] discussed about the acceleration of the transition from laminar to turbulence (boundary layer separation). Farahani et al. [77] summarised that the presence of a magnetic effect produces a Lorentz force, resulting in the generation of a strong magnetic field within the fluid flow. This leads to a faster transition from laminar to turbulent flow.

A similar outcome of $f''(c)$ and $-\theta'(c)$ is produced as in the previous analysis when the values of c are arranged differently in ascending order from $c = 0.09$ to $c = 0.10$. This phenomenon can be seen in Fig. 4, with M locked at a value of 0.01. The increase in the needle size leads to a drop in the range of $f''(c)$ and $-\theta'(c)$. The separation of the boundary layer occurs at a quicker rate when the value of c has a positive upward trend until reaching a certain level. According to Waini et al. [71], an increase in c leads to an increase in the interaction between the surface of the needle and the fluid particle. Consequently, the velocity of fluid motion rises, causing the flow separation to accelerate. In describing the type of solutions in Fig. 4, there is no solution for situations when the first and second solutions cross at λ_c and λ_c has to deal at a level lower than λ_c.

4.2. The velocity and temperature profiles

With the intention to visually illustrate the utilisation of the defined methods for constructing the dimensionless boundary conditions, as described in Eq. (10), we provide illustrative depictions in Fig. 5, Fig. 6. The analysis is conducted at constant values of Pr, ϕ, and λ using SWCNTs/water nanofluids. As we can see in Fig. 5, an increase in M can result in distinct responses to the first and second solutions. The rise in M from 0 to 0.02 can reduce the fluid velocity for the first solution.

Adversely, the second solution displays an upward trend for the velocity profile, indicating a favourable outcome. The opposite trend also can be detected for the first and second solutions for the temperature profiles. The first solution induces a growth in the temperature profile due to an increase in M. This outcome is in line with Motozawa et al.' [78] experiment. As reported by Motozawa et al. [78], the inclusion of a magnetic field into the fluid flow had a beneficial effect on the transmission of heat.

The impact of c on the velocity and temperature profiles can be illustrated in Fig. 6. The boost in c can decrease and increase the velocity and temperature profiles for the first solution, respectively. However, due to the increase in c, the second solution displays profiles that contradict the first solution.

Upon analysing Fig. 5, Fig. 6, it becomes obvious that the numerical findings gathered exhibit notable characteristics of asymptotic convergence. Based on Fig. 5, Fig. 6, we can also conclude that the first solution has a narrower profile compared to the second solution.

4.3. The physical quantities

To determine the ideal base fluid, we conduct an analysis to calculate the skin friction coefficient and the local Nusselt number for both SWCNTs/water nanofluids and SWCNTs/kerosene nanofluids. The parameter M undergoes a transition from $M = 0$ to $M = 0.2$, and the value of Pr alters from 6.2 (water) to 21 (kerosene). The value of ϕ spans from 0 to 0.1, while the other parameters remain fixed at $\lambda = 0.2$ and $c = 0.1$. The manifestation of this phenomenon is shown in Fig. 7. Fig. 7 shows that the performance of kerosene is better than that of water in both the skin friction coefficient and the local Nusselt number. Another observation is that the increment of about 15% in the skin friction coefficient and around 2% in the local Nusselt number for SWCNTs/water nanofluids and SWCNTs/kerosene nanofluids can be achieved successfully by increasing the value of M by 50%. In addition, when the value ϕ doubles, the skin friction increases by approximately 5 % and the heat transfer coefficient improves by nearly 33 %.

To compare the effectiveness of SWCNTs and MWCNTs as depicted in Fig. 8, which are both suspended in water, we manipulate the parameter of needle size within the range of $c = 0.1$ to $c = 0.3$ while maintaining a constant value of $\mathrm{Pr} = 6.2$. The effects of M and λ are kept at a value of 0.01 and 0.3, respectively. From Fig. 8, we can highlight the increase in both the skin friction coefficient and the local Nusselt number for SWCNTs/water and MWCNTs/water due to a decrease in c. The skin friction and heat transfer coefficients rise by roughly 16 % and 9 %, respectively, with a 50 % drop in thin needle size. The scenario arises because a smaller needle provides a greater surface area and hence achieves improved contact with the surrounding materials. Hence, the heat transfer rate is enhanced for smaller needle. Moreover, it has been consistently verified through Fig. 8 that SWCNTs excel over MWCNTs for both the skin friction and heat transfer coefficients.

4.4. The optimal heat transfer rate

The process of finding the optimal solutions due to the three different parameters that are mentioned in Subsection 3.2 begins with arranging a comprehensive tabulation of the factors that comprise the uppermost, intermediate, and lowermost values, as depicted in Table 5.

By replacing $F = 3$, and $C = 6$ in Eq. ((19), 20 trials are conducted for the experiment, and the data are listed in Table 6. Table 6′s data are used to conduct ANOVA to determine the experiment's significance. The results of the ANOVA are shown in Tables 7, 8.

Due to the fact that some of the sources in Tables 7, 8 have the P-value greater than 0.05, these sources are eliminated. By dropping the sources from Tables 7, 8, these tables have become the reduced model as depicted in Table 9, 10. The symbol * that displayed in Tables 7-10 indicates the value is too small to be tabulated.

After the significance test is reconducted and all resources are sufficiently satisfied based on the statistical method, the data from Tables 9, 10 become valid to be tested for optimising responses. As the statistical requirements are fulfilled, Eqs. (17) – (18) turn into expressions in order to set up the predictive model of the heat transmission rate both for SWCNTs and MWCNTs as follows:

$$y_{\mathrm{SWCNT}} = 3.62166 + 0.60676x_1 + 0.04920x_2 - 0.21935x_3 + 0.01821x_1^2 + 0.10556x_3^2 - 0.02081x_1x_3, \tag{20}$$

$$y_{MWCNT} = 3.50043 + 0.53310x_1 + 0.05142x_2 - 0.21234x_3 + 0.01657x_1^2 - 0.01143x_2^2 + 0.10487x_3^2 + 0.00696x_1x_2 - 0.01474x_1x_3. \tag{21}$$

From Eqs. (20) – (21), we can see that these models are composed of linear, interactions between parameters and have quadratic forms on the heat transfer coefficients. The interaction between parameters can be illustrated using contour plots and surface plots, as in Figs. 9-12. These models have a probability of delivering optimal solutions precisely because of their quadratic structure.

Due to the confidently performing the final step of finding optimisation, response optimiser that is supported by Minitab is applied to identify the optimum combination of parameter in order to obtain the maximum heat transfer for both SWCNTs and MWCNTs. As observed in Tables 11, 12, when the desirability function is near 100 percent (100 % for y_{SWCNT} and 99.73 % for y_{MWCNT}), the maximum heat transfer rate can be attained by setting M and ϕ to their high values, $M = 0.3$ and $\phi = 0.03$, while c is set to the low level at $c = 0.1$. Tables 11, 12 also point out that SWCNTs possess a higher heat transfer rate than MWCNTs, where this result consistently holds the argument from the numerical experiments that were performed before in Subsection 4.3.

5. Conclusion

In this present paper, the impact of MHD on the flow has been considered when investigating the CNTs nanofluids flow over a moving and horizontally slender needle. The adjustment of the significant parameters leads to the following conclusions regarding the boundary layer's and heat transfer's behaviour, physical quantities, and the optimal solution:

i. If the thin needle moves in the opposite direction, where $\lambda < -1$, then non-unique solutions are constructed.
ii. The increase in M and c reduce the range solutions $f''(c)$ and $-\theta'(c)$.
iii. When M and c decrease, it is permissible to prolong boundary separation.
iv. Increasing the value of M about 100 % in CNTs nanofluids flow can increase both skin friction and heat transfer coefficients by nearly 30 % and 4 %, respectively.
v. Lowering the value of c twofold in the flow of CNT nanofluids can increase the heat transfer coefficient by approximately 18 % and the skin friction coefficient by around 32 %.
vi. Rising 100 % in the value of ϕ can boost 5 % and 33 % of the skin friction and heat transmission coefficients.
vii. Both in terms of skin friction and heat transfer coefficients, kerosene produces superior results to water.
viii. With a close to 100 % desirability value, numerical experiments and RSM results indicate that the heat transmission coefficient of SWCNTs is greater than that of MWCNTs.
ix. The maximum value of the heat transfer rate is generated when M and ϕ are at the highest level and c is at lowest level.

We can come to the conclusion that our findings significantly contribute to the fields of mathematical analysis, thermal management, and engineering. To extend our models, it is possible to develop a three-dimensional (3D) model of CNT flow over a thin needle. Furthermore,

the numerical results provided in this model can be compared to the experimental results for a better illustration of flow and heat transfer behaviour.

Funding

1 MyBrainSc (Scholarship) from the Ministry of Higher Education Malaysia is providing financial support for completing the current work.
2 The publication fee is financially supported by Universiti Sultan Azlan Shah.

CRediT authorship contribution statement

Nazrul Azlan Abdul Samat: Conceptualization, Data curation, Formal analysis, Investigation, Methodology, Project administration, Resources, Software, Visualization, Writing – original draft, Writing – review & editing. **Norfifah Bachok:** Conceptualization, Supervision, Validation, Writing – review & editing. **Norihan Md Arifin:** Conceptualization, Supervision, Validation.

Declaration of Competing Interest

The authors declare that they have no known competing financial interests or personal relationships that could have appeared to influence the work reported in this paper.

References

[1] Reddy PS, Sreedevi P, Chamkha A, Al-Mudhaf A. Heat and mass transfer boundary layer flow over a vertical cone through porous media filled with Cu-water and Ag-water. Nanofluid Heat Trans Res 2018;49:119–43. https://doi.org/10.1615/HeatTransRes.2017016247.
[2] Reddy PS, Sreedevi P, Sheremet M. Impact of homogeneous–heterogeneous reactions on heat and mass transfer flow of Au–Eg and Ag–Eg Maxwell nanofluid past a horizontal stretched cylinder. J Therm Anal Calorim 2020;141. https://doi.org/10.1007/s10973-020-09581-3.
[3] Dinarvand S, Rostami M. Rotating Al_2O_3-H_2O nanofluid flow and heat transfer with internal heating, velocity slip and different shapes of nanoparticles. Multidiscipline Modeling in Mater Struct 2020. https://doi.org/10.1108/MMMS-01-2020-0017.
[4] Ali B, Jubair S, Fathima D, Akhter A, Rafique K, Mahmood Z. MHD flow of nanofluid over moving slender needle with nanoparticles aggregation and viscous dissipation effects. Sci Prog 2023;106(2):368504231176151. https://doi.org/10.1177/00368504231176151.
[5] Ibrahim H, Sazali N, Shah ASM, Karim MSA, Aziz F, Salleh WNW. A review on factors affecting heat transfer efficiency of nanofluids for application in plate heat exchanger. J Adv Res in Fluid Mech and Therm Sci 2019;60(1):144–54. https://www.akademiabaru.com/submit/index.php/arfmts/article/view/2636.
[6] Choi US, Eastman JA. Enhancing thermal conductivity of fluids with nanoparticles, developments and application of non-Newtonian flows. ASME J Heat Trans 1995;66:99–105.
[7] Sajid T, Tanveer S, Sabir Z, Guirao JLG. Impact of activation energy and temperature-dependent heat source/sink on Maxwell-Sutterby fluid. Math Probl Eng 2020:1–15. https://doi.org/10.1155/2020/5251804.
[8] Abbas N, Rehman KU, Shatanawi W, Abodayeh K. Mathematical model of temperature-dependent flow of power-law nanofluid over a variable stretching Riga sheet. Waves Random Complex Media 2022. https://doi.org/10.1080/17455030.2022.2111029.
[9] Awan AU, Ahammad NA, Shatanawi W, Allahyani SA, Tag-ElDin EM, Abbas N, et al. Significance of magnetic field and Darcy-Forchheimer law on dynamics of Casson-Sutterby nanofluid subject to a stretching circular cylinder. Int Commun Heat Mass Trans 2022;139:106399. https://doi.org/10.1016/j.icheatmasstransfer.2022.106399.
[10] Abbas N, Rehman KU, Shatanawi W, Al-Eid AA. Theoretical study of non-Newtonian micropolar nanofluid flow over an exponentially stretching surface with free stream velocity. Adv Mech Eng 2022;14(7). https://doi.org/10.1177/16878132221107790.
[11] Abbas N, Shatanawi W, Shatnawi T. Theoretical analysis of modified non-Newtonian micropolar nanofluid flow over vertical Riga sheet. Int J Mod Phys B 2022;37. https://doi.org/10.1142/S0217979223500169.
[12] Abbas N, Tumreen M, Shatanawi W, Qasim M, Shatnawi TAM. Thermodynamic properties of second grade nanofluid flow with radiation and chemical reaction over slendering stretching sheet. Alex Eng J 2023;70:219–30. https://doi.org/10.1016/j.aej.2023.02.031.
[13] Abbas N, Ali M, Shatanawi W, Mustafa Z. Thermodynamic properties of Second-grade micropolar nanofluid flow past an exponential curved Riga stretching surface with Cattaneo-Christov double diffusion. Alex Eng J 2023;81:101–17. https://doi.org/10.1016/j.aej.2023.09.020.
[14] Prakasha DG, Kumar KG, Saeed WS, Afzal A. Thermophoresis and Brownian motion effect on hybrid nanoparticles flow over a wedge surface by considering double stratification effects. Numerical Heat Trans Part a: App 2024. https://doi.org/10.1080/10407782.2024.2314229.
[15] Reddy PS, Sreedevi P. Impact of chemical reaction and double stratification on heat and mass transfer characteristics of nanofluid flow over porous stretching sheet with thermal radiation. Int J Ambient Energy 2022;43(1):1626–36. https://doi.org/10.1080/01430750.2020.1712240.
[16] Reddy PS, Sreedevi P, Chamka A. Heat and mass transfer flow of a nanofluid over an inclined plate under enhanced boundary conditions with magnetic field and thermal radiation. Heat Trans-Asian Res 2016;46. https://doi.org/10.1002/htj.21245.
[17] Sreedevi P, Reddy PS. Combined effects of thermophoresis and Brownian motion on three dimensional Maxwell nanofluid flow over Stretching sheet with thermal radiation and chemical reaction. J Porous Media 2020;23. https://doi.org/10.1615/JPorMedia.2020027982.
[18] Dinarvand S, Behrouz M, Ahmadi S, Ghasemi P, Noeiaghdam S, Gamiz UF. Mixed convection of thermomicropolar AgNPs-GrNPs nanofluid: an application of mass-based hybrid nanofluid model. Case Studies in Therm Eng 2023;49:103224. https://doi.org/10.1016/j.csite.2023.103224.
[19] Dinarvand S, Berrehal H, Pop I, Chamkha A. Blood-based hybrid nanofluid flow through converging/diverging channel with multiple slips effect: a development of Jeffery-Hamel problem. Int J Numer Meth Heat Fluid Flow 2022;33. https://doi.org/10.1108/HFF-08-2022-0489.
[20] Sreedevi P, Reddy PS, Rao KVS. Effect of magnetic field and radiation on heat transfer analysis of nanofluid inside a square cavity filled with silver nanoparticles: Tiwari-Das model. Waves Random Complex Media 2024;34(2):804–22. https://doi.org/10.1080/17455030.2021.1918798.
[21] Sreedevi P, Reddy PS. Effect of magnetic field and thermal radiation on natural convection in a square cavity filled with TiO_2 nanoparticles using Tiwari-Das nanofluid model. Alex Eng J 2021;61. https://doi.org/10.1016/j.aej.2021.06.055.
[22] Sreedevi P, Reddy PS. Williamson hybrid nanofluid flow over swirling cylinder with Cattaneo-Christov heat flux and gyrotactic microorganism. Waves Random Complex Media 2021:1–28. https://doi.org/10.1080/17455030.2021.1968537.
[23] Mahmood T, Ullah A, Ali R. Improved nanocomposite materials and their applications. Nanocomposite Mater Biomedical and Energy Storage App 2021. https://doi.org/10.5772/intechopen.102538.
[24] Aladag B, Halelfadl S, Doner N, Maré T, Duret S, Estellé P. Experimental investigations of the viscosity of nanofluids at low temperatures. App Energy 97 2012:876–80. https://doi.org/10.1016/j.apenergy.2011.12.101.
[25] Arya A, Sarafraz MM, Shahmiri S. Thermal performance analysis of a flat heat pipe working with carbon nanotube-water nanofluid for cooling of a high heat flux heater. Heat Mass Transf 2018;54(1):985–97. https://doi.org/10.1007/s00231-017-2201-6.
[26] Iijima S. Helical microtubules of graphitic carbon. Nature 1991;354:56–8. https://doi.org/10.1038/354056a0.
[27] Afrand M, Ranjbarzadeh R. Hybrid nanofluids preparation method. Hybrid Nanofluids for Convection Heat Transfer 2020:49–99. https://doi.org/10.1016/B978-0-12-819280-1.00002-1.
[28] Ali N, Bahman AM, Aljuwayhel NF, Ebrahim SA, Mukherjee S, Alsayegh A. Carbon-based nanofluids and their advances towards heat transfer applications–a review. Nanomaterials 2021;11(6):1628. https://doi.org/10.3390/nano11061628.
[29] Yasir M, Ahmed A, Khan M. Carbon nanotubes-based fluid flow past a moving thin needle examine through dual solutions: stability analysis. J Storage Mater 2022;48(6430):103913. https://doi.org/10.1016/j.est.2021.103913.
[30] Lee LL. Boundary layer over a thin needle. Phys Fluids 1967;10:820–2. https://doi.org/10.1063/1.1762194.
[31] Souayeh B, Reddy MG, Sreenivasulu P, Poornima T, Mohammad RG, Alarifi IM. Comparative analysis on non-linear radiative heat transfer on MHD Casson nanofluid past a thin needle. J Mol Liq 2019;284:163–74. https://doi.org/10.1016/j.molliq.2019.03.151.
[32] Shafiq A, Colak AB, Sindhu TN. Designing artificial neural network of nanoparticle diameter and solid–fluid interfacial layer on single-walled carbon nanotubes/ethylene glycol nanofluid flow on thin slandering needles. Int J Numer Meth Fluids 2021;93(12):3384–404. https://doi.org/10.1002/fld.5038.
[33] Kumar JP, Umavathi JC, Dhone AS. Forced convection of magnetohydrodynamic (MHD)–boundary layer flow past thin needle with variable wall temperature using Casson nanofluid. J Nanofluids 2023;12:271–9. https://doi.org/10.1166/jon.2023.1998.
[34] Tlili I, Ramzan M, Kadry S, Kim HW, Nam Y. Radiative MHD nanofluid flow over a moving thin needle with entropy generation in a porous medium with dust particles and Hall current. Entropy 2020;22(3):354. https://doi.org/10.3390/e22030354.
[35] Singh P, Kumar D, Kumari A. Effect of heat and mass transfer in nanofluid flow along a vertical thin needle. Mater Today: Proc 2022;57:2276–80. https://doi.org/10.1016/j.matpr.2021.12.574.
[36] Gul T, Ullah MZ, Ansari KJA, Amiri IS. Thin film flow of CNTs nanofluid over a thin needle surface. Surf Rev Lett 2020;27(8):1950189. https://doi.org/10.1142/S0218625X19501890.
[37] Afridi MI, Tlili I, Qasim M. Nonlinear Rosseland thermal radiation and energy dissipation effects on entropy generation in CNTs suspended nanofluids flow over a thin needle. Bound Value Problems 2018;148. https://doi.org/10.1186/s13661-018-1062-3.

[38] Sreedevi P, Reddy PS. Impact of convective boundary condition on heat and mass transfer of nanofluid flow over a thin needle filled with carbon nanotubes. J Nanofluids 2020;9(4):282–92. https://doi.org/10.1166/jon.2020.1751.
[39] Nayak M, Mabood F, Dogonchi AS, Khan W. Electromagnetic flow of SWCNT/MWCNT suspensions with optimized entropy generation and cubic auto-catalysis chemical reaction. Int Commun Heat Mass Transfer 2020;120(1):104996. https://doi.org/10.1016/j.icheatmasstransfer.2020.104996.
[40] Bharat BB, Barai DP. Thermophysical properties of nanofluids. Nanofluids for Heat and Mass Transfer, Academic Press; 2021. p. 101–66.
[41] Salleh SNA, Zin NAM, Najib N. Verification of dual solutions for water and kerosene-based carbon nanotubes over a moving slender needle. Symmetry 2022;14:2306. https://doi.org/10.3390/sym14112306.
[42] Olia H, Torabi M, Bahiraei M, Ahmadi MH, Goodarzi M, Safaei MR. Application of nanofluids in thermal performance enhancement of parabolic trough solar collector: state-of-the-art. Appl Sci 2019;9:463. https://doi.org/10.3390/app9030463.
[43] Anuar NS, Bachok N, Arifin NM, Rosali H. Role of multiple solutions in flow of nanofluids with carbon nanotubes over a vertical permeable moving plate. Alex Eng J 2020;59(12):763–73. https://doi.org/10.1016/j.aej.2020.02.015.
[44] Samat NAA, Bachok N, Arifin NM. Carbon nanotubes (CNTs) nanofluids flow and heat transfer under mhd effect over a moving surface. J Adv Res Fluid Mech Therm Sci 2023;103(1):165–78. https://doi.org/10.37934/arfmts.103.1.165178.
[45] Aziz A, Sidik NAC, Rahman S, Asako Y, Yusof SNA. A review of passive methods in microchannel heat sink application through advanced geometric structure and nanofluids: current advancements and challenges. Nanotechnol Rev 2020;9:1192–216. https://doi.org/10.1515/ntrev-2020-0094.
[46] Ibrahim W, Tulu A. Magnetohydrodynamic (MHD) boundary layer flow past a wedge with heat transfer and viscous effects of nanofluid embedded in porous media. Hindawi Mathematical Problems in Eng 2019:1–12. https://doi.org/10.1155/2019/4507852.
[47] Ahmad S, Yousaf M, Khan A, Zaman G. Magnetohydrodynamic fluid flow and heat transfer over a shrinking sheet under the influence of thermal slip. Heliyon 2018;4(10). https://doi.org/10.1016/j.heliyon.2018.e00828.
[48] Salleh SNA, Bachok N, Arifin NM, Ali FM, Pop I. Magnetohydrodynamics flow past a moving vertical thin needle in a nanofluid with stability analysis. Energies 2018;11:3297. https://doi.org/10.3390/en11123297.
[49] Salleh SNA, Bachok N, Arifin NM, Ali FM. A stability analysis of solutions on boundary layer flow past a moving thin needle in a nanofluid with slip effect. ASM Sc J 2019;12(1):60–70. https://www.akademisains.gov.my/asmsj/article/a-stability-analysis-of-solutions-on-boundary-layer-flow-pasta-moving-thin-needle-in-a-nanofluid-with-slip-effect/.
[50] Aladdin NAL, Bachok N, Rosali H, Wahi N, Rahmin NAA, Arifin NM. Numerical computation of hybrid carbon nanotubes flow over a stretching/shrinking vertical cylinder in presence of thermal radiation and hydromagnetic. Mathematics 2022;10:3551. https://doi.org/10.3390/math10193551.
[51] Mabood F, Muhammad T, Nayak MK, Waqas H, Makinde OD. EMHD flow of non-Newtonian nanofluids over thin needle with Robinson's condition and Arrhenius pre-exponential factor law. Phys Scr 2020;95:115219. https://doi.org/10.1088/1402-4896/abc0c3.
[52] Khan A, Saeed A, Tassaddiq A, Gul T, Kumam P, Ali I, et al. Bio-convective and chemically reactive hybrid nanofluid flow upon a thin stirring needle with viscous dissipation. Sci Rep 2021;11:8066. https://doi.org/10.1038/s41598-021-86968-8.
[53] Khan WA, Khan ZH, Rahi M. Fluid flow and heat transfer of carbon nanotubes along a flat plate with Navier slip boundary. Appl Nanosci 2014;4:633–41. https://doi.org/10.1007/s13204-013-0242-9.
[54] Dinarvand S, Berrehal H, Tamim H, Sowmya G, Noeiaghdam S, Abdollahzadeh M. Squeezing flow of aqueous CNTs-Fe_3O_4 hybrid nanofluid through mass-based approach: Effect of heat source/sink, nanoparticle shape, and an oblique magnetic field. Results in Eng 2023;17:100976. https://doi.org/10.1016/j.rineng.2023.100976.
[55] Alahmadi RA, Raza J, Mushtaq T, Abdelmohsen SA, Gorji MR, Hassan AM. Optimization of MHD flow of radiative micropolar nanofluid in a channel by RSM: sensitivity Analysis. Mathematics 2024;11:939. https://doi.org/10.3390/math11040939.
[56] Asshaari I, Jedic A, Hamzah FM. Magnetohydrodynamic boundary layer in carbon nanotube past a moving plat with slip and thermal radiation effect. Jurnal Kejuruteraan SI 2022;5(2):91–9. https://doi.org/10.17576/jkukm-2022-si5(2)-10.
[57] Samat NAA, Bachok N, Arifin NM. The significant effect of hydromagnetic on carbon nanotubes based nanofluids flow and heat transfer past a porous stretching/shrinking sheet. J Adv Res in Fluid Mech Therm Sci 2023;106(1):51–64. https://doi.org/10.37934/arfmts.106.1.5164.
[58] Xue QZ. Model for thermal conductivity of carbon nanotube-based composites. Phys B Condens Matter 2005;368(1–4):302–7. https://doi.org/10.1016/j.physb.2005.07.024.
[59] Oztop HF, Abu-Nada E. Numerical study of natural convection in partially heated rectangular enclosures filled with nanofluids. Int J Heat Fluid Flow 2008;29(5):1326–36. https://doi.org/10.1016/j.ijheatfluidflow.2008.04.009.
[60] Dinarvand S, Yousefi M, Chamkha AJ. Numerical simulation of unsteady flow toward a stretching/shrinking sheet in porous medium filled with a hybrid nanofluid. J App Computational Mech 2022;8(1):11–20. https://doi.org/10.22055/jacm.2019.29407.1595.
[61] Aladdin NAL, Bachok N, Pop I. Boundary layer flow and heat transfer of Cu-Al_2O_3/water over a moving horizontal slender needle in presence of hydromagnetic and slip effects. Int Commun Heat Mass Trans 2021;123(1):105213. https://doi.org/10.1016/j.icheatmasstransfer.2021.105213.
[62] Roy U, Roy PK. Chapter 7 - Advances in heat intensification techniques in shell and tube heat exchanger. In: Advanced Analytic and Control Techniques for Thermal Systems with Heat Exchangers. Academic Press; 2020. p. 197–207. https://doi.org/10.1016/B978-0-12-819422-5.00007-4.
[63] Abbas N, Shatanawi W, Shatnawi TAM. Thermodynamic study of radiative chemically reactive flow of induced MHD sutterby nanofluid over a nonlinear stretching cylinder. Alex Eng J 2023;70:179–89. https://doi.org/10.1016/j.aej.2023.02.038.
[64] Khan U, Zaib A, Shah Z, Baleanu D, Sherif ESM. Impact of magnetic field on boundary-layer flow of Sisko liquid comprising nanomaterials migration through radially shrinking/stretching surface with zero mass flux. J Mater Res Technol 2020;9(3):3699–709. https://doi.org/10.1016/j.jmrt.2020.01.107.
[65] Ali UK. Solution of BVPs using bvp4c and bvp5c of MATLAB. Boundary Value Problems for Eng 2019:417–510. https://doi.org/10.1007/978-3-030-21080-9_10.
[66] Lamidi S, Olaleye ON, Oluremi YO, Bankole A, Obalola E, Aribike AI. Applications of response surface methodology (RSM) in product design, development, and process optimization. Response Surf Methodology - Res Adv App 2022. https://doi.org/10.5772/intechopen.106763.
[67] Mahanthesh B, Mackolil J, Mallikarjunaiah M. Response surface optimization of heat transfer rate in Falkner-Skan flow of ZnO EG nanoliquid over a moving wedge: Sensitivity analysis. Int Commun Heat Mass Trans 2021;125:105348. https://doi.org/10.1016/j.icheatmasstransfer.2021.105348.
[68] Jawairia S, Raza J. Optimization of heat transfer rate in a moving porous fin under radiation and natural convection by response surface methodology: sensitivity analysis. Chem Eng J Adv 2022;1:100304. https://doi.org/10.1016/j.ceja.2022.100304.
[69] Yahaya RI, Mustafa MS, Arifin NM, Pop I, Ali FM, Isa SSPM. Hybrid nanofluid flow past a biaxial stretching/shrinking permeable surface with radiation effect: stability analysis and heat transfer optimization. Chin J Phys 2023;85:402–20. https://doi.org/10.1016/j.cjph.2023.06.003.
[70] N.A.A. Samat, N., N.M. Arifin, Boundary layer stagnation point flow and heat transfer over a nonlinear stretching/shrinking sheet in hybrid carbon nanotubes: numerical analysis and response surface methodology under the influence of magnetohydrodynamics, Computation, 12 (2024) 46, DOI: 10.3390/computation12030046.
[71] Waini I, Ishak A, Pop I. On the stability of the flow and heat transfer over a moving thin needle with prescribed surface heat flux. Chin J Phys 2019;60:651–8. https://doi.org/10.1016/j.cjph.2019.06.008.
[72] Ibrar N, Reddy MG, Shehzad SA, Sreenivasulu P, Poornima T. Interaction of single and multi-walls carbon nanotubes in magnetized-nano Casson fluid over radiated horizontal needle. SN App Sci 2020;2:677. https://doi.org/10.1007/s42452-020-2523-8.
[73] Sharma BR, Konwar H. MHD flow, heat and mass transfer due to axially moving cylinder in presence of thermal diffusion, radiation and chemical reactions in a binary fluid mixture. Int J Computer App 2015;110(15):52–9. https://doi.org/10.5120/19396-1074.
[74] Rehman KU, Shatanawi W, Malik MY. Heat transfer and double sampling of stratification phenomena in non-Newtonian liquid suspension: a comparative thermal analysis. Case Studies in Therm Eng 2022;33:101934. https://doi.org/10.1016/j.csite.2022.101934.
[75] Zhou X, Jiang Y, Wang Y, Jiang Y, Huang H. Comprehensive heat transfer performance analysis of liquid metal based nanofluid laminar flow in circular tube. Int J Mech Sci 2020;175(2):105530. https://doi.org/10.1016/j.ijmecsci.2020.105530.
[76] Kraszewska A, Donizak J. An analysis of a laminar-turbulent transition and thermal plumes behavior in a paramagnetic fluid subjected to an external magnetic field. Energies 2021;7972 (10.3390/en14237972).
[77] Farahani SD, Amiri M, Majd BK, Mosavi A. Effect of magnetic field on heat transfer from a channel: nanofluid flow and porous layer arrangement. Case Studies Therm Eng 2021;28:101675. https://doi.org/10.1016/j.csite.2021.101675.
[78] Motozawa M, Chang J, Sawada T, Kawaguchi Y. Effect of magnetic field on heat transfer in rectangular duct flow of a magnetic fluid. Phys Procedia 2010;9:190–3. https://doi.org/10.1016/j.phpro.2010.11.043.

Nazrul Azlan Abdul Samat Nazrul Azlan Abdul Samat is currently a doctoral student in the Department of Mathematics, Faculty of Science at Universiti Putra Malaysia (UPM) in Malaysia. He is also an academic staff member at Universiti Sultan Azlan Shah (USAS) in Malaysia. He completed his Master's Degree in Scientific Computation with Industrial Mathematics at the University of Nottingham, United Kingdom. Previously, he did his first degree in mathematics at UPM. He participated in several international conferences, majoring in applied mathematics and engineering. In addition, he made significant contributions to various publications that are indexed in Scopus, including studies on the boundary layer flow of carbon nanotubes and heat transfer.

Dr. Norfifah Bachok Dr. Norfifah Bachok is currently an Associate Professor in the Department of Mathematics, Faculty of Science at Universiti Putra Malaysia (UPM) in Malaysia. She is also an associate researcher in the Institute of Mathematical Research at UPM. She obtained her PhD from Universiti Kebangsaan Malaysia (UKM). She received her master's degree and first degree from Universiti Putra Malaysia (UPM). In addition to her

academic career, she held several managerial positions. Her proficiency in fluid dynamics and applied mathematics is recognised in scholarly publications such as those published by Elsevier and Springer with 5821 citations, 39 h-index, and 97 i10-index.

Prof. Dr. Norihan Md Arifin Prof. Dr. Norihan Md. Arifin is currently a Professor and Head of Department in the Department of Mathematics, Faculty of Science at Universiti Putra Malaysia (UPM) in Malaysia. She obtained her PhD from Universiti Kebangsaan Malaysia (UKM). She was awarded a master's degree from the University of Strathclyde and the Glasgow Caledonian, United Kingdom, and a first degree from Universiti Putra Malaysia (UPM). Her main research interests are fluid mechanics and heat transfer, especially when it comes to thermal convection and boundary-layer theory. She also studies heat transfer in Newtonian and non-Newtonian fluids, as well as fluid-saturated porous media and nanofluids. She has contributed to more than 60 technical papers with 5829 citations, 39 h-index, and 155 i10-index.